# HIGH PRESSURE SURFACE ENHANCED RAMAN SCATTERING SPECTROSCOPY

BY

YUANXI FU

DISSERTATION

Submitted in partial fulfillment of the requirements
for the degree of Doctor of Philosophy in Chemistry
in the Graduate College of the
University of Illinois at Urbana-Champaign, 2015

Urbana, Illinois

Doctoral Committee:

Professor Dana Dlott, Chair
Professor Jay Bass
Professor Martin Gruebele
Professor Steve Granick

## ABSTRACT

Surface-enhanced Raman scattering spectroscopy (SERS) was combined with the diamond anvil cell technique to study molecular monolayers and single molecules under high pressure. Vibrational spectra up to 8 GPa were obtained for self-assembled monolayers (SAMs) of the energetic material simulant 4-nitrobenzenethiol (NBT). A large pressure-broadening $NO_2$ symmetrical stretch was found in the SAMs but not in solid NBT. Single-molecule Raman spectra were studied at high pressures (1-4 GPa). The molecules were two isotopologues of the dye rhodamine 6G (R6G and $d_4$-R6G), adsorbed on colloidal Ag particles immobilized in polyvinyl alcohol (PVA). The distributions of pressure-induced blueshifts and linewidths of individual molecules were obtained at different pressures. The linewidth of the single-molecule Raman spectra increased little with pressure, but the variations in blueshifts increased significantly and accounted for most of the pressure-broadening found in the ensemble Raman spectra. To study the pressure effect on plasmon-based electromagnetic enhancement, localized surface plasmon resonance (LSPR) spectra of a photonic substrate and Raman scattering spectra of bezenethiol (BT) monolayers adsorbed upon were measured simultaneously under high pressure. The LSPR split into two peaks under initial compression, and both peaks redshifted with further-increased pressure. The shifts in LSPR was correlated to the Raman intensity variations found in BT Raman spectra. These results suggest that both deformation in the nanoparticles and changes in the dielectric functions with pressure should be taken into account when designing SERS substrates intended for working at high pressures.

*To my parents*

# ACKNOWLEDGEMENTS

I am grateful to my advisor Professor Dana Dlott for his support and guidance to my research, particularly in the high pressure single-molecule Raman study. I would like to thank Professor Jay Bass for his generous help with the diamond anvil cell, Professor Martin Gruebele for insightful discussions regarding research and teaching, and Professor Steve Granick for correspondence at the beginning, heartfelt conversations in between, and a job offer at the end. I would like to thank all the Dlott group members, former and current, particularly Dr. Kathryn Brown for teaching me the technique of surface enhanced Raman spectroscopy and diamond anvil cell. Dr. Brown carried out the first high-pressure SERS measurement and therefore laid down the foundation upon which this piece of work was developed. I would like to thank Dr. Natalia Garcia-Rey and Dr. Prabudahha Mukherjee for teaching me the technique of vibrational sum frequency generation spectroscopy. I appreciate Dr. Dianwen Zhang from the Microscope Suite at Beckman Institute of Science and Technology for his assistance with the confocal Raman microscope system. Finally, I want to thank my parents and friends for love and support.

Works presented were supported by supported by US Air Force Office of Scientific Research under award number FAA9550-09-1-0163, and Defense Threat Reduction Agency under award HDTRA1-12-1-0011. I am grateful to Professor Richard P. Van Duyne of Northwestern University for giving us the d4-R6G and a great deal of useful advice.

# TABLE OF CONTENTS

# LIST OF FIGURES

# LIST OF TABLES

# CHAPTER 1: INTRODUCTION

## 1.1 Motivations

With the advent of advanced experimental techniques and theories, the field of high-pressure research has witnessed rapid growth since the early 20$^{th}$ century. One major objective of high-pressure research is to measure the structure and property of materials under high pressure, generating valuable data for many disciplines of science and engineering. In addition, because high pressure is capable of inducing structural transformations, predicting and producing high-pressure phases and novel materials comprises another research focus [1-5].

High pressure can be generated via dynamics or statics compression. Dynamics compression techniques include light-gas gun, laser-driven shock, flyer plate, and ramp compression [6], whereas static pressure generation involves usage of devices such as the diamond-anvil cell [7] and multi-anvil apparatus [8].

The diamond anvil cell (DAC) is the most widely used device for generating static high pressure. It produces the highest static pressure due to the unrivaled hardness of diamond. Gem-quality diamonds can be transparent to x-ray, ultraviolet, visible and infrared radiation (except in the range of 2 to 7 μm) [9]. DAC can thus be integrated with many spectroscopic techniques. The major drawback of DAC is the small sample volume, which can be overcome by using brighter radiation sources and more sensitive detectors.

Raman scattering spectroscopy utilizes the frequency shifts of photons that occur when they encounter molecular vibrations. It has been applied to study materials under high pressure since the advent of DAC [7], and it is particularly useful in identifying pressure-induced phase transitions [10-13].

Raman spectra under high pressure generally exhibit blueshifts and broadenings [14-19]. The blueshifts occur as a consequence of reduced inter-atomic spacing and anharmonicity in the interaction potentials [18]. Broadening originates from many sources, however, and is often described as homogeneous or inhomogeneous. Homogeneous broadening of vibrational transitions in solids arises primarily from "pure dephasing" caused by faster modulations of the vibrational frequency by the surroundings [20-24], whereas inhomogeneous broadening results from each molecule in the ensemble having different interactions with the surroundings.

Raman scattering was once difficult to measure due to weak signals. Its utility was restricted until the advent of lasers, better detectors, and band-rejection filters. The subsequent discovery of the surface enhancement effect significantly elevated the sensitivity of Raman scattering spectroscopy [25]. The enhancement mainly comes from collected electron oscillations on metal surfaces, so-called localized surface plasmon resonance (LSPR) [26]. Excitation of LSPR with lasers amplifies the electromagnetic fields near the metal surfaces and thus enhances the Raman scattering signal of affected molecules by $10^4$ to $10^{10}$ [27-29]. With such large enhancement, single-molecule detection using Raman scattering became possible [30,31].

Applying surface-enhanced Raman scattering spectroscopy (SERS) to high-pressure research opens a handful of opportunities. The number of molecules required to make detectable signal is reduced accordingly, allowing Raman studies that range from molecular monolayers to single molecules. By definition, single-molecule Raman spectra should be purely homogeneously broadened [32,33]. Therefore, single-molecule Raman spectroscopy permits the responses of the individual molecules that constitute inhomogeneous pressure-broadening to be resolved.

## 1.2 Organization

This thesis focuses on the study of high-pressure SERS spectra of molecules adsorbed on metal surfaces, with three objectives to achieve: to compare the compressed state of surface molecules to their crystalline counterparts; to observe single-molecule Raman scattering under high pressure; and to examine the pressure response of localized surface plasmon resonance (LSPR).

Chapter 2 gives a brief overview of surface-enhanced Raman scattering (SERS) spectroscopy.

Chapter 3 documents the experimental apparatus and operating procedure of DAC.

Chapter 4 includes work that examines the vibrational response of 4-nitrobenzenethiol (NBT) self-assembled monolayers (SAM) and solids under high pressure. It was found that the blueshifts of monolayer and solid were similar except for the anchoring C-S group, confirming previous findings in studies of benzenethiol and methyl-benzenethiol. The similarity was attributed to the mobility of surface molecules, which causes the monolayer to compress along three dimensions rather than one dimension if the molecules were stationary. A significant pressure broadening was found in the $NO_2$ symmetrical stretch in SAM but not in the solid. The broadening was attributed to the rearrangement that had randomized nitro group orientations.

Chapter 5 covers a high-pressure single-molecule SERS study of Rhodamine 6G adsorbed on Ag colloidal nanoparticles that were immobilized in a poly-vinyl alcohol film. A dramatic loss of Raman intensity was found when the samples were first put under pressure. This intensity loss was not caused by pressure tuning of the R6G absorption spectrum but by pressure reduction of plasmonic enhancement of the SERS-active hotspots. Analysis of datasets in which

single-molecule spectra dominated showed that the single-molecule Raman linewidths increased very little due to increasing pressure, but the variations in the pressure-induced single-molecule blueshifts increased significantly with pressure. Therefore, individual single molecules can have quite different pressure-shifting behavior, and the variations in blueshifts among single R6G molecules explained the pressure-induced broadening.

Chapter 6 includes work that examined the pressure response of the LSPR of a photonic substrate, namely Ag film over nanospheres (AgFON). The nanosphere array LSPR was centered at ~620 nm at ambient pressure. When it was placed under moderate pressure, however, it split into two resonances, centering at ~500 nm and ~750 nm, respectively; this was presumably caused by deformations of the polymer nanoparticles. Both resonances redshifted with increasing pressure. In accordance to the LSPR splitting and shifting, SERS intensity increased by twofold at 2 GPa but decreased gradually from 2 to 10 GPa. These results suggest that both deformation in the nanoparticles and changes in the dielectric functions with pressure should be taken into account when designing SERS substrates intended for working at high pressures.

### 1.3 References


[1] N.W. Ashcroft, Phys. Rev. Lett. 21 (1968) 1748.

[2] A.R. Oganov, A.O. Lyakhov, M. Valle, Acc. Chem. Res. 44 (2011) 227.

[3] Y. Tian, B. Xu, D. Yu, Y. Ma, Y. Wang, Y. Jiang, W. Hu, C. Tang, Y. Gao, K. Luo, Z. Zhao, L.-M. Wang, B. Wen, J. He, Z. Liu, Nature 493 (2013) 385.

[4] Y. Wang, Y. Ma, J. Chem. Phys. 140 (2014).

[5] W. Zhang, A.R. Oganov, A.F. Goncharov, Q. Zhu, S.E. Boulfelfel, A.O. Lyakhov, E. Stavrou, M. Somayazulu, V.B. Prakapenka, Z. Konôpková, Science 342 (2013) 1502.

[6] D.D. Dlott, Annu. Rev. Phys. Chem. 62 (2011) 575.

[7] W.A. Bassett, High Pressure Res. 29 (2009) 163.

[8] R.C. Liebermann, High Pressure Res. 31 (2011) 493.

[9] A.M. Zaitsev, Optical properties of diamond : a data handbook, Springer, Berlin, New York, 2001.

[10] S.K. Deb, M. Wilding, M. Somayazulu, P.F. McMillan, Nature 414 (2001) 528.

[11] F. Decremps, J. Pellicer-Porres, A.M. Saitta, J.-C. Chervin, A. Polian, Phys. Rev. B 65 (2002) 092101.

[12] P. Perlin, C. Jauberthie-Carillon, J.P. Itie, A. San Miguel, I. Grzegory, A. Polian, Phys. Rev. B 45 (1992) 83.

[13] S.H. Tolbert, A.P. Alivisatos, Annu. Rev. Phys. Chem. 46 (1995) 595.

[14] M. Hanfland, H. Beister, K. Syassen, Phys. Rev. B 39 (1989) 12598.

[15] S.K. Satija, B. Swanson, J. Eckert, J.A. Goldstone, J. Phys. Chem. 95 (1991) 10103.

[16] M.I.M. Scheerboom, J.A. Schouten, Phys. Rev. E 51 (1995) R2747.

[17] U.D. Venkateswaran, A.M. Rao, E. Richter, M. Menon, A. Rinzler, R.E. Smalley, P.C. Eklund, Phys. Rev. B 59 (1999) 10928.

[18] G. Lucazeau, J. Raman. Spectrosc. 34 (2003) 478.

[19] R.J. Hemley, Annu. Rev. Phys. Chem. 51 (2000) 763.

[20] L.A. Hess, P.N. Prasad, J. Chem. Phys. 72 (1980) 573.

[21] K.S. Schweizer, D. Chandler, J. Chem. Phys. 76 (1982) 2296.

[22] C.L. Schosser, D.D. Dlott, J. Chem. Phys. 80 (1984) 1394.

[23] A. Tokmakoff, D. Zimdars, B. Sauter, R.S. Francis, A.S. Kwok, M.D. Fayer, J. Chem. Phys. 101 (1994) 1741.

[24] A. Tokmakoff, M.D. Fayer, Acc. Chem. Res. 28 (1995) 437.

[25] C.L. Haynes, A.D. McFarland, R.P.V. Duyne, Analytical Chemistry 77 (2005) 338 A.

[26] M. Moskovits, J. Chem. Phys. 69 (1978) 4159.

[27] Y. Fang, N.-H. Seong, D.D. Dlott, Science 321 (2008) 388.

[28] E.C. Le Ru, P.G. Etchegoin, M. Meyer, J. Chem. Phys. 125 (2006) 13.

[29] G.C. Schatz, M.A. Young, R.P. Van Duyne, Surface-Enhanced Raman Scattering: Physics and Applications 103 (2006) 19.

[30] K. Kneipp, Y. Wang, H. Kneipp, L.T. Perelman, I. Itzkan, R.R. Dasari, M.S. Feld, Phys. Rev. Lett. 78 (1997) 1667.

[31] S. Nie, S.R. Emory, Science 275 (1997) 1102.

[32] P.G. Etchegoin, E.C. Le Ru, Analytical Chemistry 82 (2010) 2888.

[33] C. Artur, E.C. Le Ru, P.G. Etchegoin, J. Phys. Chem. Lett. 2 (2011) 3002.

# CHAPTER 2: SURFACE ENHANCED RAMAN SCATTERING SPECTROSCOPY

## 2.1 History

Surface enhanced Raman scattering was discovered in 1974, when unexpectedly large Raman scattering signal from pyridine adsorbed on roughened silver electrode was reported [1-3]. Debate over the origin of the enhancement lasted a few years till 1978. Moskovits firstly proposed that the enhancement arose from collected electron oscillations at the metal/dielectric boundary, later named localized surface plasmon resonance (LSPR) [4]. He modeled the rough electrode surface as layers of metal microspheres atop a flat metal substrate and calculated the corresponding absorption maxima $\lambda_R$ based on this model. Using $\lambda_R$ as the resonant frequency, he successfully reproduced the wavelength-dependency of the SERS intensity obtained from experiments.

A second enhancement mechanism is the "chemical enhancement", which result from amplified molecular polarization due to charge transfer between molecules and metal surfaces [5]. However, the chemical enhancement is small ($\sim 10^2$) compared to the electromagnetic enhancement ($10^4$ ~$10^{10}$), and the consensus is that the electromagnetic enhancement based on LSPR gives most important contribution to SERS.

As the origin of the enhancement was identified, fundamental studies and applications of SERS took off in the next three decades. LSPR can be calculated numerically on given nanoparticles' geometries [6]. Optimal surface enhancement was found when frequency of LSPR resided between the frequency of the excitation photon and the frequency of the scattered photon [7,8]. The magnitude of the SERS enhancement resulted from EM enhancement has been quantified as between $10^4$ to $10^{10}$ [9,10]. Sites with exceptionally high enhancement were named

"SERS hotspot" and located at the junction between nanoparticles [11]. On the application side, various types of the SERS active substrate were developed, and SERS is increasingly used in chemical sensing and biological imaging [12-14].

A modified version of SERS, tip-enhanced Raman scattering (TERS) utilizes the highly confined and enhanced electromagnetic field at the apex of a STM tip. TERS demonstrated ~0.5 nm spatial resolution [15]. It is one of the most promising avenues being pursued currently to realize real-time imaging of chemical reactions [16].

**2.2 Single-molecule surface enhanced Raman scattering (SMSERS)**

In 1997, two groups reported observation of surface enhanced Raman scattering signal from a single molecule [17,18]. As pointed out by one of the reports, single molecule SERS was only possible if the SERS enhancement could bridge the gap between the Raman scattering cross-section ($10^{-30}$ $cm^{-2}$) and fluorescence cross-section ($10^{-16}$ $cm^{-2}$). The authors believed that $10^{14}$ Raman enhancement existed at specific sites (SERS hotspots) [18].

However, the Raman enhancement of R6G on Ag nanoparticles is not solely from the metal surface, because R6G molecules absorb strongly at 532nm and therefore induces resonant Raman enhancement. The resonance Raman scattering cross-section of R6G was measured to be $2.3 \times 10^{-22}$ $cm^{-2}$ using femto-second stimulated Raman scattering [19], and surface contribution was estimated to be $10^{7}$ to $10^{8}$ [19]. On the other hand, AFM imaging of SM-SERS active particles suggested that the hotspots located at the junctions between two aggregated particles [11]. The EM enhancement of small (a few nm) gaps in between silver or gold nano-sphere dimers was theoretically investigated by Schatz and coworkers [20]. Their studies demonstrated EM enhancement as high as $10^{10}$ at the junctions. Nevertheless, structures such as triangles were

found to provide EM enhancement of similar magnitude. SM-SERS without utilizing gap junctions was demonstrated lately [21].

Since EM enhancement is site-dependent, and positioning one molecule precisely at a hotspot is so far technically unrealistic, an observed Raman spectra can either originate from a single molecule adsorbed at a hotspot or many molecules on sites with less enhancement. Isotope edited bi-analyte method (BiAS) was thus devised to identify single molecule events in SM-SERS studies [22,23]. It is implemented as the following. The analyte molecule is deuterated so that one at least one vibrational mode shifts in frequency and is separated from the undeuterated one. The purpose of deuteration is to maximally retain resonant Raman cross section and interactions with the surface between the two species. Equal amount of the two analytes are added to the nanoparticle suspension to freely associate with the particles. In a captured Raman spectrum, if both transitions appears, the spectrum cannot originate from a single-molecule. However, if the spectrum contains only one of the two transitions, it is likely to be a single molecule spectra.

### 2.3 The surface chemistry of Lee-Meisel Ag colloids

The surfaces of Lee-Miesel Ag colloidal particles carry negative surface charges due to adsorbed citrate anions. Changes in the surface charges affect the stability and SERS enhancement of the colloids [24]. The colloidal solution is stabilized by strong coulomb repulsions between negatively charged particles, and this coulomb repulsion can be screened by adding an electrolyte. Based on this principle, salt (KCl or NaCl) solution (~10 mM) induces mild aggregations of the nanoparticle, a pre-requisite for SMSERS [25]. However, small clusters

of particles are formed, but further aggregation is prevented by coulomb blocking, leading to meta-stable colloidal solutions [26].

On the other hand, R6G, a cationic dye, adsorbs onto the negatively charged Ag colloids via electrostatic interactions. The interaction was found to be so strong that free dye molecules were quickly depleted by surrounding colloidal particles before they can diffuse far [27].

The surface chemistry must be taken into account in sample preparation. Dye solution need to be prepared at least in the same volume as the colloidal solution, so that when the two solutions are mixed, dye molecules will be uniformly distributed among the particles and not induce particle aggregations [27,28]. Secondly, when the surface coverage of citrate ions are sufficiently high, their Raman signal become observable [29]. Therefore, the Ag colloid need to be treated with low concentration (~1mM) salt solution, so that the citrate adlayer is substituted by $Cl^-$ adlayer, which maintains the surface charge but is Raman-inactive.

### 2.4 High pressure surface enhanced Raman spectroscopy: previous studies

Kathryn Brown, a former group member, was the first to combined diamond anvil technique with surface enhancement Raman scattering and obtained Raman scattering spectra of self-assembled molecular monolayers (SAMs) under high pressure [30]. The SAMs she studied were benzenethiol (BT) and benzenemethylthiol (BMT), and the SERS-active substrates utilized were Ag coated nano-sphere arrays (AgFON). She found that the pressure-induced vibrational blue shifts are remarkably similar between SAMs and solids.

Lately high pressure SERS has attracted some attention from the high pressure community for its potential in amplifying weak optical signals under high pressure. A group at Jilin University studied the localized surface plasmon resonance of gold nanoparticles in a

diamond anvil cell up to 1.2 GPa [31]. Within this pressure range, the size, shape and permittivity of gold nanparticles (40 and 80nm) changed insignificantly. They found a continuous redshifts with pressure in gold nano-particle LSPR. The redshifts were correlated to the increased refractive index of water, which is used as the pressure transmission medium.

Similar study has not been conducted on silver nanoparticles. However, there are x-ray characterizations of bulk and nanoparticles of silver under high pressure. At ambient pressure, silver adopts face-centered-cubic (fcc) structure. Bulk silver retains fcc structure up to 120 GPa [32] without any identified phase transition. However, silver nanoparticles behave differently. Nanoparticles between 5 to 10 nm were found to be primarily multiply twinned icosahedral particles. Unlike cubic structure that has isotropic compressibility, at the twin boundaries, the compressibility were found to be different along different axis, leading to a reversible rhombohedral distortion [33].

**2.5 References**


[1] M.G. Albrecht, J.A. Creighton, J. Am. Chem. Soc. 99 (1977) 5215.

[2] M. Fleischmann, P.J. Hendra, McQuilla.Aj, Chem. Phys. Lett. 26 (1974) 163.

[3] D.L. Jeanmaire, R.P. Vanduyne, J. Electroanal. Chem. 84 (1977) 1.

[4] M. Moskovits, J. Chem. Phys. 69 (1978) 4159.

[5] P. Kambhampati, A. Campion, Surf. Sci. 427–428 (1999) 115.

[6] G.C. Schatz, M.A. Young, R.P. Van Duyne, Surface-Enhanced Raman Scattering: Physics and Applications 103 (2006) 19.

[7] C.L. Haynes, R.P. Van Duyne, J. Phys. Chem. B 107 (2003) 7426.

[8] A.D. McFarland, M.A. Young, J.A. Dieringer, R.P. Van Duyne, J. Phys. Chem. B 109 (2005) 11279.

[9] Y. Fang, N.-H. Seong, D.D. Dlott, Science 321 (2008) 388.

[10] E.C. Le Ru, E. Blackie, M. Meyer, P.G. Etchegoin, J. Phys. Chem. C 111 (2007) 13794.

[11] A.M. Michaels, Jiang, L. Brus, J. Phys. Chem. B 104 (2000) 11965.

[12] J. Kneipp, H. Kneipp, B. Wittig, K. Kneipp, Nanomed.-Nanotechnol. Biol. Med. 6 (2010) 214.

[13] D. Drescher, J. Kneipp, Chem. Soc. Rev. 41 (2012) 5780.

[14] C.L. Haynes, C.R. Yonzon, X. Zhang, R.P. Van Duyne, J. Raman Spectrosc. 36 (2005) 471.

[15] R. Zhang, Y. Zhang, Z.C. Dong, S. Jiang, C. Zhang, L.G. Chen, L. Zhang, Y. Liao, J. Aizpurua, Y. Luo, J.L. Yang, J.G. Hou, Nature 498 (2013) 82.

[16] J.M. Klingsporn, M.D. Sonntag, T. Seideman, R.P. Van Duyne, J. Phys. Chem. Lett 5 (2013) 106.

[17] K. Kneipp, Y. Wang, H. Kneipp, L.T. Perelman, I. Itzkan, R.R. Dasari, M.S. Feld, Phys. Rev. Lett. 78 (1997) 1667.

[18] S. Nie, S.R. Emory, Science 275 (1997) 1102.

[19] S. Shim, C.M. Stuart, R.A. Mathies, ChemPhysChem 9 (2008) 697.

[20] J.M. McMahon, S. Li, L.K. Ausman, G.C. Schatz, J. Phys. Chem. C 116 (2011) 1627.

[21] A.B. Zrimsek, A.-I. Henry, R.P. Van Duyne, J. Phys. Chem. Lett 4 (2013) 3206.

[22] J.A. Dieringer, R.B. Lettan, K.A. Scheidt, R.P. Van Duyne, J. Am. Chem. Soc. 129 (2007) 16249.

[23] E.C. Le Ru, M. Meyer, P.G. Etchegoin, J. Phys. Chem. B 110 (2006) 1944.

[24] R.A. Alvarez-Puebla, E. Arceo, P.J.G. Goulet, J.J. Garrido, R.F. Aroca, J. Phys. Chem. B 109 (2005) 3787.

[25] P. Hildebrandt, M. Stockburger, J. Phys. Chem. 88 (1984) 5935.

[26] M. Meyer, E.C. Le Ru, P.G. Etchegoin, J. Phys. Chem. B 110 (2006) 6040.

[27] B.L. Darby, E.C. Le Ru, J. Am. Chem. Soc. 136 (2014) 10965.

[28] M. Futamata, Y. Yu, T. Yajima, J. Phys. Chem. C 115 (2011) 5271.

[29] M. Kerker, O. Siiman, L.A. Bumm, D.S. Wang, Appl. Opt. 19 (1980) 3253.

[30] K.E. Brown, D.D. Dlott, J. Phys. Chem. C 113 (2009) 5751.

[31] Y. Bao, B. Zhao, D. Hou, J. Liu, F. Wang, X. Wang, T. Cui, J. Appl. Phys. 115 (2014).

[32] Y. Akahama, H. Kawamura, A.K. Singh, Journal of Applied Physics 95 (2004) 4767.

[33] K.J. Koski, N.M. Kamp, R.K. Smith, M. Kunz, J.K. Knight, A.P. Alivisatos, Physical Review B 78 (2008) 165410.

# CHAPTER 3: EXPERIMENTAL

## 3.1 Homebuilt Raman apparatus

Figure 3.1 shows the layout of our homebuilt Raman apparatus. The laser was a 30 mW, 532nm doubled Nd:$YVO_4$. Laser output power was attenuated to 1 mW for Raman scattering measurements and focused down to ~30 μm spot. Ruby chips in the DAC were excited by the same laser. Raman and fluorescence spectra were detected by a Shamrock 303i spectrograph (Andor) with a PIXIS 256 CCD camera (Princeton instruments). The spectral resolution was 10 $cm^{-1}$. The reflectance spectra of the nano-sphere arrays and the extinction spectra of the Ag nanoaggregates were used to determine the LSPR spectra. The samples were illuminated by a Tungsten-Halogen lamp (Ocean optics, HL-2000), and the LSPR spectra were acquired by a miniature spectrometer (Ocean Optics USB4000). The sample inside DAC is imaged using a video camera (National Instrument) to facilitate the experiment.

## 3.2 Confocal Raman microscope

For SMSERS studies, two types of instrumentations exist. In one of them, laser illuminates an area that is larger than the field of view of the objective. Raman active spots can be identified in the field of view as diffraction-limited spots. Each individual diffraction-limited spot is centered on the entrance slit of the spectrograph to collect Raman spectra [1,2]. The advantage of this instrumentation is that SERS active spot is selected before its spectra is taken, ensuring the successful capture of SMSERS spectra. However, such instrumentation is highly customized for carrying out SMSERS studies, and only exists as home-built versions.

The second type of instrumentation utilizes confocal Raman imaging microscope [3], and is adopted in this study. Compared to the conventional Raman spectrometer, confocal Raman

microscope blocks off-focus scattering by positioning in front of the detector a pinhole that is confocal with the illumination spot, an;d therefore improves the spatial resolution. To put it in another way, the scattering volume from which the Raman signal is collected is much more restricted in a confocal Raman microscope than in a conventional Raman spectrometer. The advantage is easy implementation, because confocal Raman microscope is commercially available. Yet the spectra acquisition process is blind and inefficient: Raman spectra are taken point-by-point without knowing whether the laser illumination or the pinhole is optimally aligned with a given SERS active spot.

The confocal Raman microscope used is a Horiba LabRAM HR confocal Raman imaging microscope. The objective was a Nikon long-working distance 50X objective with N.A. = 0.5. The laser power was attenuated to 0.1 mW at 532 nm and 0.6 mW at 633nm for Raman scattering measurement. The confocal pinhole diagonal was 300 μm, and the spectrograph slit width was 200 μm. The diffraction grating was 1800 g/mm, blazed at 500 nm.

A slab of high refractive index material such as a diamond anvil between the objective and specimen can introduce aberrations and enlarge the observed scattering volume [4,5]. To characterize the effects of our 2.5 mm thick diamond anvil, we measured the scattering volume with and without the diamond anvil using a method [6] from the literature. The measured scattering volume in air was 30 $\mu m^3$, and with the diamond anvil the scattering volume was enlarged to 81 $\mu m^3$. However the samples were only 20 μm thick, which limited the actual axial detection depth to the sample thickness. In that situation, we estimated the scattering volume to be 25 $\mu m^3$. Parameters used to calculate the scattering volume are listed in Table 3.1.

### 3.3 Diamond anvil cell

Diamond anvil cell (DAC) is a convenient device to subject small specimen (0.01 $mm^3$) to high pressures (GPa to TPa). Since diamonds are transparent from UV to far infrared (moderate absorptions between 2 to 7 microns), DAC can be easily adapted to laser Raman spectroscopy. The Raman active lattice mode of diamond appears at 1332 $cm^{-1}$. It comes from the vibrations of the two interpenetrating cubic sublattices of the diamond against one another [7]. Nitro symmetrical stretching mode, a transition of interest to us (1345 $cm^{-1}$) overlaps with the diamond lattice mode. In that case, SiC anvils were used.

By bring two opposing anvils to close contact and applying moderate force on the tables, high pressure are generated at the culet (tip). Various design of DAC were proposed to implement this simple idea, emphasizing on either adapting the DAC to a certain analytical technique or achieving higher pressure. The DAC used in this study was a Merril-Basset type cell [8].

A metal (BeCu or stainless steel) gasket in between the two opposing anvils encloses the specimen, the pressure transmission medium and ruby chips for pressure determination. The diameter of the sample hole was chosen to be between ½ to ⅔ of the culet diameter. Before drilling the hole, the gaskets must be pre-indented to a thickness between 50 to 100 μm [9].

The pressure transmission medium transforms uniaxal compression to hydrostatic compression. Choices include rare gases, organic liquids and salt. Ar was used in this study. It was cryogenically loaded into a DAC according to the following procedures. The assembled DAC was placed into a brass chamber. The chamber was purged with dry Ar and then placed into a liquid nitrogen bath. When chamber reached equilibrium, Ar gas was slowly flowed into the chamber, condensed on the wall and flew into the DAC. Once the liquid Ar was above the

top surface of DAC, the three DAC screws were tightened to slightly beyond pre-draw marker to trap the Ar in the sample chamber.

The pressure in a diamond anvil cell is determined by ruby R1 line shifts. When a $Cr^{3+}$ ion replaces an $Al^{3+}$ ion in $\alpha$-$Al_2O_3$ lattice, the $Cr^{3+}$ ion is under the influence of an octahedral ligand field formed six surrounding $O^{2-}$ ions that breaks the degeneration of the five d orbitals. Ruby $R_1$ (694.25 nm) and $R_2$ (692.68nm) line are emissions from two $^2E$ levels [10]. Hydrostatic pressure isotropically deforms $Al_2O_3$ lattice. The crystal field splitting scales reversely with the forth power of metal-ligand bond length. Changes in the field splitting lead to the shifts of the Ruby R1 and R2 lines that are proportional to pressure [11]. The center frequency of R1 line is converted to pressure using calibration equation provided in reference [12].

### 3.4 Sample preparation: Ag film over nanospheres (AgFON)

The nano-array substrate was a 15 μm Mylar® film whose surface was made hydrophilic with a sputtered coating of 25 nm of $SiO_2$. A drop of aqueous suspension of 320 nm polystyrene spheres (Thermo Scientific) was evaporated on the surface to form a close-packed nanosphere lattice, and 200 nm of Ag were sputtered onto the nanospheres. The sphere diameter and Ag thickness were those that optimize the array for 532 nm laser Raman scattering. The SAM was deposited by soaking the array in a 1mM solution of thiol (benzenthiol or 4-nitrobenzenthiol, Sigma-Aldrich) in ethanol for several hours. A scalpel was used to slice a tiny piece of the array that fit into the anvil.

### 3.5 Sample preparation: dye treated Ag nanoparticle immobilized in polymer film

The citrate-reduced Ag colloid samples were prepared according to Lee and Meisel's method [13]. The colloid solution (20 mL) was mixed with an equal quantity of aqueous solution of R6G [14]. The R6G was rhodamine 590 chloride (Exciton), and the $d_4$-R6G was provided to us by Prof. Van Duyne of Northwestern University. By trial and error, we found the best R6G concentrations were 30 nM of each isotopologue for the lower-pressure studies. At higher pressures where the number of hot spots was smaller, we used 60 nM. Combined citrate and R6G solutions were vortexed for 30 s. Then 40 mL of 20 mM NaCl solution were added, followed by another 30 s of vortexing to assist nanoparticle aggregation. The suspensions were incubated for 1.5 hour. To remove R6G in solution, the suspension was centrifuged at 10,000 rpm for 15 minutes. The precipitate was mixed with 20 mL 0.5mM NaCl and dispersed by vortexing. This process was repeated until the R6G concentration in the supernatant dropped below 1nM, as assessed by fluorescence. The precipitate collected from the final centrifugation was mixed with 1.6 g of 5% poly vinyl alcohol (PVA) (J. T. Baker, MW 77,000-79,000) in water. This mixture was drop-coated onto a 2"×2" glass plate cleaned by Piranha solution ($H_2SO_4$: $H_2O_2$ = 3:1), and then air-dried to form a greenish-yellow film ~20 μm thick. The film on glass was inserted into the SERS spectrometer, and regions were located that produced the strongest SERS signals. Using a scalpel and a microscope, sample chips approximately 200 x 200 x 20 $\mu m^3$ were cut from those regions.

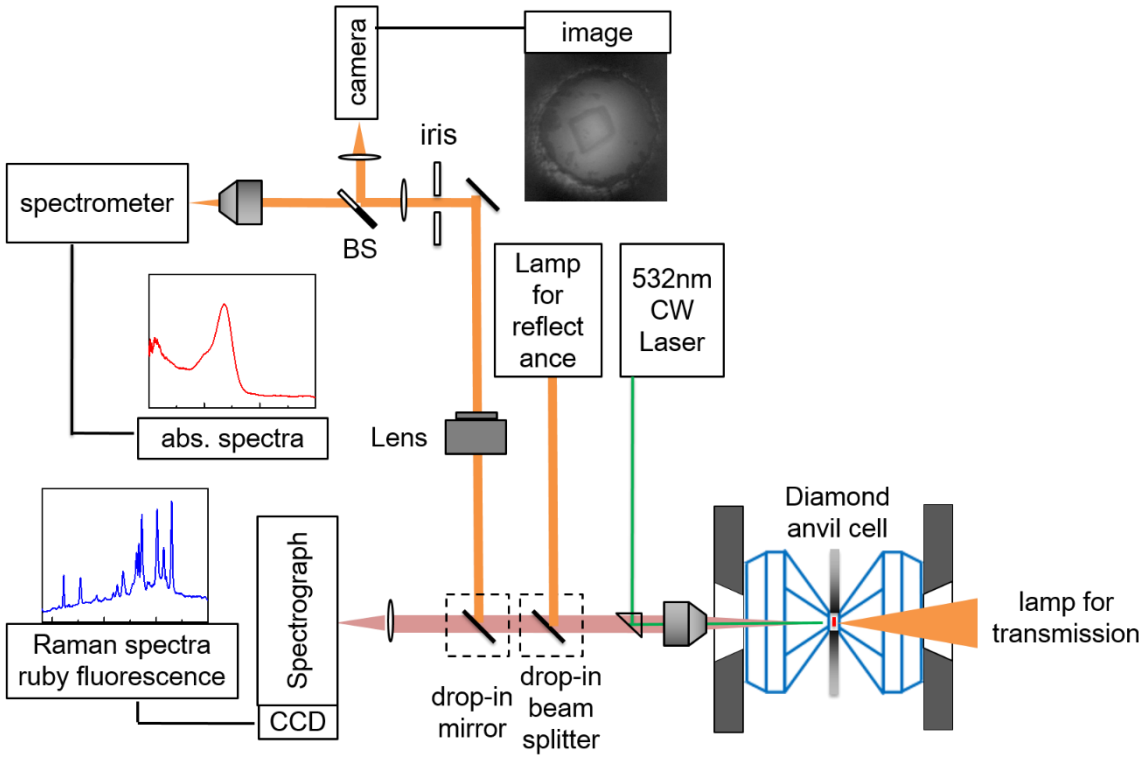


**Figure 3.1**

Layout of the homebuilt Raman apparatus.

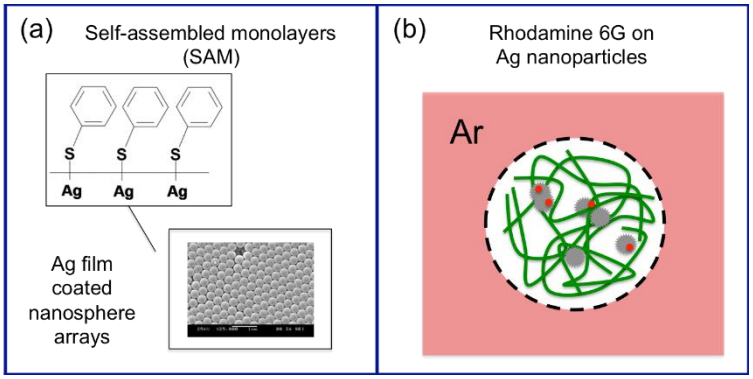


**Figure 3.2**

Schematics of two SERS active samples that had been studied in DAC under high pressure. (a) Self-assembled monolayer on a photonic substrate consisting of an Ag-coated nano-sphere array. (b) R6G dye (red dots) adsorbed on Ag nanoparticle aggregates (grey) immoblized in a PVA matrix (green).

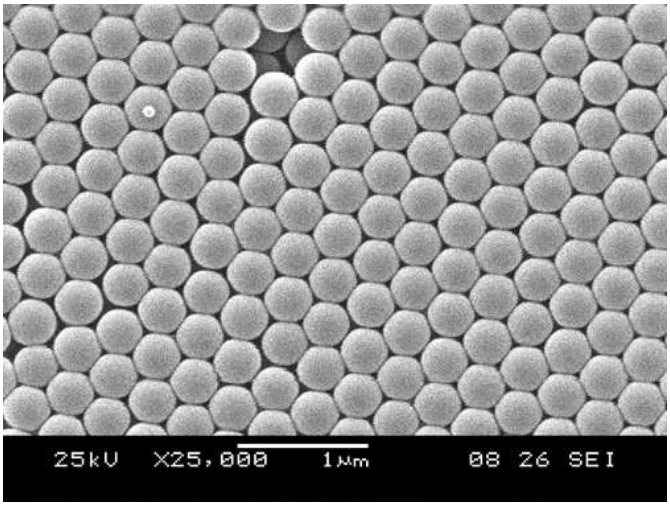


**Figure 3.3**

Scanning electron microscope image of the nano-sphere arrays.

| configuration | $\omega_0$ (μm) | $H_{eff}$ (μm) | $V_{eff}$ (μm$^3$) |
|---|---|---|---|
| in air | 0.9 | 24 | 30 |
| through the diamond window | 0.9 | 64 | 81 |
| on the film sample | 0.9 | 20* | 25 |

***** The thickness of the film sample

**Table 3.1**

Parameters for calculating the scattering volume

### 3.6 References


[1] J.A. Dieringer, R.B. Lettan, K.A. Scheidt, R.P. Van Duyne, J. Am. Chem. Soc. 129 (2007) 16249.

[2] S.M. Stranahan, K.A. Willets, Nano Letters 10 (2010) 3777.

[3] E.C. Le Ru, E. Blackie, M. Meyer, P.G. Etchegoin, J. Phys. Chem. C 111 (2007) 13794.

[4] K.J. Baldwin, D.N. Batchelder, Appl. Spectrosc. 55 (2001) 517.

[5] N.J. Everall, Analyst 135 (2010) 2512.

[6] E.C. Le Ru, E. Blackie, M. Meyer, P.G. Etchegoin, J. Phys. Chem. C 111 (2007) 13794.

[7] G. Eckhardt, D.P. Bortfeld, M. Geller, Applied Physics Letters 3 (1963) 137.

[8] L. Merrill, W.A. Bassett, Rev. Sci. Instrum. 45 (1974) 290.

[9] D.J. Dunstan, Rev. Sci. Instrum. 60 (1989) 3789.

[10] Y. Tanabe, S. Sugano, J. Phys. Soc. Jpn. 12 (1957) 556.

[11] K. Syassen, High Pressure Res. 28 (2008) 75.

[12] H.K. Mao, J. Xu, P.M. Bell, Journal of Geophysical Research: Solid Earth 91 (1986) 4673.

[13] P.C. Lee, D. Meisel, J. Phys. Chem. 86 (1982) 3391.

[14] B.L. Darby, E.C. Le Ru, J. Am. Chem. Soc. 136 (2014) 10965.

# CHAPTER 4: VIBRATIONAL SPECTROSCOPY OF NITROAROMATIC SELF-ASSEMBLED MONOLAYERS UNDER EXTREME CONDITIONS*

## 4.1 Introduction

Nitro groups are a key functionality of most high-performance energetic materials (EM), and vibrational spectroscopy of nitro groups under dynamic shock compression [1-5] can be an important method for understanding fundamental mechanisms of EM initiation. Interpreting vibrational spectra under shock conditions can pose several problems. For example the net shock-induced frequency shift may result from opposing pressure blueshift and temperature redshift [6]. In this study we investigate the vibrational spectra of nitro groups of the EM simulant 4-nitro-benzenethiol (NBT) under static high-pressure (to 8 GPa) and high-temperature (to ~600°C). The NBT simulant was studied in both the crystalline form ('solid') and as a self-assembled monolayer ('SAM') on polycrystalline Au or Ag (111) surfaces (Fig. 4.1a). The relevance of SAMs for ultrafast shock compression measurements stems from the fact that shock velocities in EM are a few nanometers per picosecond. The time resolution of shock compression measurements is limited by the shock front transit time across the sample layer being probed, so monolayers will yield the highest possible time resolution [7].

One difficulty in monolayer studies arises from the small quantity of molecules being probed. We have overcome this in flash-heating and shock compression experiments using a nonlinear coherent vibrational spectroscopy termed broadband multiplex sum-frequency generation (SFG) [7,8]. In static high-pressure experiments we have developed a photonic chip

* Materials in this chapter have been previously published in following article: Fu, Yuanxi; Friedman, Elizabeth A.; Brown, Kathryn E.; Dlott, Dana D. Chem. Phys. Lett, 2011, 501, 369-374. Copyright © Elsevier, reprint with permission.

that can be placed in a diamond-anvil cell (DAC), to amplify the Raman signal of a SAM by about one million using the surface-enhanced Raman scattering (SERS) effect (Fig. 4.1b) [9].

A pertinent difficulty in studying EM at high temperatures stems from the fast thermochemical reactivity. We have overcome this difficulty by femtosecond laser flash-heating, where the SAM's metallic substrate is heated by many hundreds of K. Due to the thin film geometry, the T-jump decays by thermal conduction on the nanosecond time scale. The nanosecond duration of the heat pulse applied to the SAM effectively suppresses chemical decomposition [8,10].

There have been a few vibrational spectroscopy studies of nitrated EM under shock compression [1-5] and quite a few studies with static high pressure (e.g. [11,12]). Some of these studies involved poly-nitro EM such as TATB (1,3,5-triamino-2,4,6 trinitrobenzene) [13], which featured a number of complications such as inter- and intra-molecular interactions among multiple nitro groups, extensive hydrogen bonding and solid-solid phase transitions, which will not be discussed here. The mono-nitro compounds nitromethane (NM) [14-20] and nitrobenzene (NB) [21-24] have been studied by Raman under static and dynamic compression. These materials have a symmetric nitro stretch transition $\nu^s NO_2$ prominent in the Raman spectrum near 1400 $cm^{-1}$ (NM) or 1345 $cm^{-1}$ (NB). In NM, which decomposes under pressure at ~150°C [15], $\nu^s NO_2$ has been studied in a DAC up to 35 GPa at 20° and 80°C [17,18]. The pressure dependent blueshift is ~2 $cm^{-1}$ $GPa^{-1}$, although there are breaks in slope due to phase transitions [17,18]. Unfortunately, Raman spectroscopy of shocked NM did not tell us much about $\nu^s NO_2$ specifically, because the measurements did not resolve $\nu^s NO_2$ from nearby $\nu^s CH_3$ transitions [19]. Shock compression measurements of NB showed that the $\nu^s NO_2$ transition had the smallest blueshift of any of the more intense Raman transitions and this smaller blueshift was ~1.2 $cm^{-1}$

$GPa^{-1}$. The small blueshift was explained as resulting from an offsetting redshift due to pressure-induced changes in the intermolecular interactions [21].

In comparing shock to static spectroscopy measurements it is useful to keep in mind that a shock is more than just high pressure and high temperature. Shocks launched by tabletop femtosecond lasers are typically quasi-1D with rise-times of a few picoseconds and durations of 10-100 ps [25,26]. As depicted in Fig. 4.2a, with such shocks molecules initially are subjected to uniaxial stress, which creates a longitudinal strain (i.e. along the shock propagation axis) and a shear stress [27]. If the shear stress $\sigma$ exceeds a critical value $\sigma_{cr}$, which depends on material strength, then a subsequent shear relaxation [28,29] will occur. The shear relaxation causes the uniaxial strain to decay as the transverse expansion occurs, leading to a final state of hydrostatic compression. The shear relaxation may not be complete, however, and the final state may not be quite hydrostatic, if the shocked material possesses residual strength characterized by a nonzero value of $\sigma_{cr}$ [27].

A femtosecond laser-driven shock front also excites molecules via multi-phonon up-pumping [30-32]. In up-pumping, the front creates an initial non-equilibrium vibrational population dominated by doorway-mode excitations. Doorway modes are lower-frequency larger-amplitude vibrations that have larger mode-Grüneisen parameters. The Grüneisen parameter characterizes the rate of increase of vibrational energy with volume compression. The initial doorway-rich vibrational population causes a vibrational redistribution process that excites the other vibrations, leading to a thermalized state at an elevated temperature on the 10-100 ps time scale [30,31]. Following shear and vibrational relaxation processes, the shocked molecules will be approximately (to the extent that $\sigma_{cr} \approx 0$) in an equilibrium state of elevated pressure and temperature.

Thus to better interpret shock vibrational spectroscopy experiments, it would be useful to have independent measurements of molecular spectra under conditions of hydrostatic compression and high temperature. For EM, nitro-group spectra are particularly important. But in addition it would be useful to have measurements with uniaxial compression only and with non-equilibrium vibrational populations. In this study we report progress toward those goal.

## 4.2 Experimental

NBT was obtained from Aldrich Chemical Company and used without further purification. The static high-pressure Raman measurements used the scheme described in Chapter 2. We used Moissanite (SiC) rather than diamond anvils, because the diamond Raman transition overlaps the $\nu^{s}NO_2$ symmetric stretching transition near 1345 $cm^{-1}$. Raman spectra were obtained with both increasing and decreasing pressures but no hysteresis was observed.

The flash-heating apparatus with nonresonant suppression was also described in detail previously [10]. A Cr-Au thin film on glass with adsorbed NBT SAM was flash-heated to a high temperature in the 600°C range by femtosecond pulses [10]. A femtosecond IR pulse centered near 1345 $cm^{-1}$ and a picosecond 800 nm pulse were used to obtain SFG spectra as a function of time delay after flash-heating. The spectroscopic resolution was 11 $cm^{-1}$.

## 4.3 Results

Figure 4.1c shows Raman spectra of the NBT SAM and solid at a lower pressure of 0.2 GPa, with some selected peak assignments. Four transitions were studied in detail, selected because they were not spectrally congested and had sufficient Raman intensities. These were the CS-stretch υCS, the CN-stretch υCN, the symmetric nitro stretch $\upsilon^{s}$ $NO_2$, and the totally-

symmetric in-plane ring stretch υ8a. Figure 4.3 compares SERS and solid-state spectra up to 7 GPa. Figure 4.4 shows the pressure-dependent blueshifts. Except for νCS, the shifting behavior was almost identical for SAM and solid, which was also the case in a previous study of benzenethiol [9].

It is useful to know the mode Grüneisen parameter γ for each transition, where γ is the relative change in wavenumber ν with respect to the relative change in volume V,

$$\gamma = \frac{\partial ln\bar{\nu}}{\partial lnV} \qquad (1)$$

Unfortunately the quantity we determine is the relative rate of energy change with pressure, $d$ lnν / $dP$ , and to convert this quantity to γ would require a knowledge of the isothermal compressibility $\kappa = -(d\ln V/dP)_T$ for the SAM, which we do not know. In any case the values in Table 4.1 for a single substance should be indicative of the relative magnitudes of the mode Grüneisen parameters. For the νCS determination we used the lower-pressure (< 3 GPa) slope of the SERS data in Fig. 4.4a. The important conclusion is that $d$ lnν / $dP$ is about the same for $\nu NO_2$, $\nu^s$ NO2 and ν8a, but it is about ten times larger for νCS. A comparison to other SAMs is also possible. The ν8a transition was studied in BT and benzene-methyl-thiol SAMs [9], and its pressure-dependent blueshift was almost identical to the NBT results in Fig. 4.4d. As seen in Fig. 4.1c, the Raman linewidths are narrower in the solid. Figure 4.5 compares the pressure-dependent Raman linewidths of $\nu^s$ $NO_2$ and ν8a. The ν8a linewidth does not change appreciably with pressure in the solid or the SAM. The $\nu^s$ $NO_2$ linewidth increases significantly in both solid and SAM, but the pressure dependences are quite different. In the SAM the linewidth increases by about a factor of five up to 3 GPa and then levels off. In the solid the linewidth does not increase much until ~4 GPa. Figure 4.6 compares the $\nu^s$ $NO_2$ transition of the NBT SAM with hydrostatic compression and with flash-heating. The ambient spectra were obtained with both

SERS and SFG. In the SFG spectra the non-resonant signal from the Au substrate was suppressed using time-gating [33,34]. The NBT flash-heating data are in good agreement with a previous study surveying many SAM structures [10]. Although SFG and Raman are quite different techniques, the $\nu^s$ $NO_2$ spectra are similar. The peak locations are close but the Raman has a ~15% greater width. The SFG spectrum is narrower because the SFG cross-section is the product of the IR and Raman cross-sections [33], in the dipole approximation with non-resonant susceptibility suppressed.

Figure 4.6 shows that flash-heating to 600°C causes a small redshift of ~1 $cm^{-1}$ and negligible broadening. This is true at shorter (2 ps) time delay when non-equilibrium vibrational populations are present [10], and at longer (80 ps) time delay when NBT and the substrate are in equilibrium at 600°C. High pressure causes a significant blueshift of ~15 $cm^{-1}$ and a FWHM increase from 20 $cm^{-1}$ to 70 $cm^{-1}$.

## 4.4 Discussions

### 4.4.1 Pressure-dependent spectra

Besides the usual pressure-dependent blueshifts, there are three features in Figs. 4.3-5 worth additional remarks. The first is the similarity between the pressure shift of SAM and solid for νCN, $\nu^s$ $NO_2$ and ν8a (Figs. 4.4b-d). The second is the unusual behavior of νCS in Fig. 4.4a. In the SAM, νCS blueshifts up to 3 GPa and then stops, whereas in the solid there is almost no shift at all. Since the CS linkage is part of the SAM anchor to its substrate, the pressure shift is suggestive of an ad-layer structural relaxation in the 0-3 GPa range not present in the solid. The third is the behavior of the solid NBT ν8a ring stretch mode in Fig. 4.3. A relatively sharp (FWHM 14 $cm^{-1}$) band at lower pressures, at ~5 GPa a weaker broader (FWHM ~100 $cm^{-1}$)

feature appears on its red edge. With increasing pressure this broader feature blueshifts on top of the ν8a peak, stealing its intensity. We suggest the broader feature is the asymmetric nitro stretch transition $\nu^a$ $NO_2$ which would be expected to be weak in the Raman spectrum. In this view, pressure tuning creates a Fermi resonance with ν8a, leading to intensity redistribution and broadening.

### 4.4.2 Structural relaxation

The similarities of the pressure shift data for NBT SAM and solid can be viewed as surprising, since the SAM is anchored to a metal substrate. The same result was obtained in an earlier comparison of BT SAM and solid at high pressure [9]. This pressure shift result can be explained as follows.

Solid NBT in the Ar pressure medium would be expected to undergo a hydrostatic but somewhat anisotropic compression, based on static compression measurements of the closely related solid, NB [22]. At the higher pressures used here (e.g. 6 GPa), NB solid undergoes volume compression of ~25% [22]. According to x-ray data, NB crystals at 6.1 GPa compress by 14%, 4% and 10% along the a, b and c-axes respectively [22].

NBT SAMs consist of molecules adsorbed on a comparatively incompressible metal substrate. With sudden ~6 GPa hydrostatic compression, a SAM would first be compressed only along the surface normal [9], as depicted in Fig. 4.2b. (With dynamic diamond anvil technology, sample could be loaded to 6 GPa in 10 ms [35].) This uniaxial response could, in principle, occur on a molecular time scale (picoseconds) [7], and the uniaxial strain would be ~25% at 6 GPa. Because molecular force constant tensors are highly anisotropic, the Raman spectrum of a

SAM with a solely uniaxial compression SAM would be quite different from an isotropically compressed solid.

However organic thiolates on noble metal surfaces are known to have a sluggish surface mobility, which is necessary for them to form highly-ordered monolayers [36]. Thiolate SAMs can also be pushed around a metal surface by an AFM tip [37]. Thus we propose that the initial uniaxial strain undergoes a gradual shear relaxation when the shear stress overcomes the SAM adhesion to the substrate. The adhesion determines $\sigma_{cr}$. As illustrated in Fig. 4.2b, the shear relaxation resulting from hydrostatic compression would be a compression process, as opposed to the shear expansion (Fig. 4.2a) that would result from shock compression. We do not see the proposed uniaxial state or the shear relaxation because the relaxation apparently occurs faster than the several minutes needed for us to compress the sample and obtain spectra. It might be observable in the future using dynamically-actuated [35] DACs.

The CS-stretching transition νCS should be especially sensitive to the nature of SAM packing on surface. The νCS shift is minimal in the solid (Fig. 4.4a), but in the SAM there is a blueshift of ~7 cm-1GPa-1 up to ~3 GPa. Thus the shift data is suggestive of a shear-induced rearrangement on the surface up to ~3 GPa. Above 3 GPa the SAM becomes practically incompressible for stress parallel to the surface plane.

### 4.4.3 Doorway modes

A steep shock front preferentially pumps energy into molecular vibrations at a rate proportional to the mode Grüneisen parameter [31]. Looking at the data in Table 4.1, in the SAM the CS-stretch transition νCS would be expected to be shock-excited an order of magnitude more efficiently than the nitro stretch or ring vibrations. Thus the νCS vibration can be considered a

doorway mode for shock-to-molecule energy transfer in the SAM. However this is apparently not true for solid NBT, where the CS-linkage does not serve as a molecular support.

### 4.4.4 Nitro SAM spectra at high pressure and temperature

Figure 4.6 shows that flash-heating results in small thermal redshifts and broadening of the SAM $\nu^s$ $NO_2$ transition. In condensed media, the thermal redshift and broadening are frequently dominated by thermal expansion [38], but these flash-heating measurements are faster than thermal expansion. Another likely mechanism involves quartic anharmonic coupling between a higher-frequency vibration being observed, such as $\nu^s$ $NO_2$, and unobserved lower-frequency vibrations near kT [39]. Energy exchange between the lower-frequency vibrations and the bath cause a fluctuating anharmonic shift of the observed vibration that results in a redshift and broadening having identical temperature dependences proportional to the thermal occupation number of the lower-frequency mode [39].

Figure 4.5 also shows that static high pressure causes the SAM $\nu^s$ $NO_2$ transition to blueshift, and this blueshift is about the same as in the solid. Thus it is reasonable to associate the $\nu^s$ $NO_2$ pressure blueshift with intramolecular anharmonicity. Increasing strain causes the $\nu^s$ $NO_2$ ground-state $\nu = 0$ to move up in energy, but the excited-state $\nu = 1$ energy moves up to an even greater extent.

The SAM $\nu^s$ $NO_2$ transition broadens significantly in a pressure range (0-3GPa) where the solid NBT linewidth is insensitive to pressure. At the same time the SAM phenyl $\nu$8a transition hardly broadens at all. These observations lead us to associate the broadening with the nitro group location at the interface between the SAM and the Ar pressure medium. A likely hypothesis, supported by the similarity between the $\nu$CS pressure blueshift (Fig. 4.4a) and the $\nu^s$

$NO_2$ broadening (Fig. 4.5a), involves the proposed shear relaxation process described in Fig. 4.1b.

During shear relaxation the SAM molecules move in the plane to become more tightly packed, which requires the surface nitro groups to be dragged through the Ar pressure medium. This rearrangement creates a distribution of nitro group orientations. The disordered nitro groups create static inhomogeneous broadening. Another possibility, suggested by the observation that vacuum deposition of metal films on top of SAMs can lead to metal atoms being embedded within the SAM [40,41], is that the inhomogeneous broadening is caused by Ar atoms in the SAM lattice. However we regard this as less likely [9] because SAMs because, although there are strong interactions between organic molecules and metal atoms, organic molecules such as benzene are totally immiscible in Ar.

### 4.4.5 Relationships between static and dynamic shock-compression spectra

The flash-heating results show that the $\nu^s$ $NO_2$ transition of the SAM, on shorter time scales relevant to shock compression, is insensitive to high temperatures up to 600°C and additionally insensitive to the non-equilibrium vibrational distributions created at the earlier stages of flash-heating. Thus we would expect the static and shock blueshifts to be similar at a given pressure, since the shock pressure blueshift will not be appreciably offset by a temperature redshift. This could potentially be a useful simplification, since the shock pressure could then be determined in situ with reference to static high-pressure calibration measurements.

According to our hypothesis for the origin of the pressure broadening for $\nu^s$ $NO_2$ of the SAM, the broadening is associated with the shear relaxation process. This could be another potentially useful simplification where the initial uniaxial compression would be associated with

a sudden blueshift with minimal broadening and the subsequent shear relaxation by a subsequent gradual broadening.

## 4.5 Conclusions

Vibrational spectra up to 8 GPa and 600 °C were obtained for self-assembled monolayers (SAMs) on noble metal surfaces of the energetic material simulant 4-nitrobenzenethiol (NBT). The high-pressure measurements used a surface-enhanced Raman sensor. The high-temperature measurements used femtosecond laser flash-heating and nonlinear coherent vibrational spectroscopy. The SAM nitro stretching transition ($\nu^s$ $NO_2$) is insensitive to flash-heating where there is no time for chemical reactivity or thermal expansion. A large pressure broadening in $\nu^s$ $NO_2$ of the SAM but not in solid NBT was associated with surface ad-layer rearrangement. The implications for time-resolved measurements of shock-compressed energetic materials are discussed.

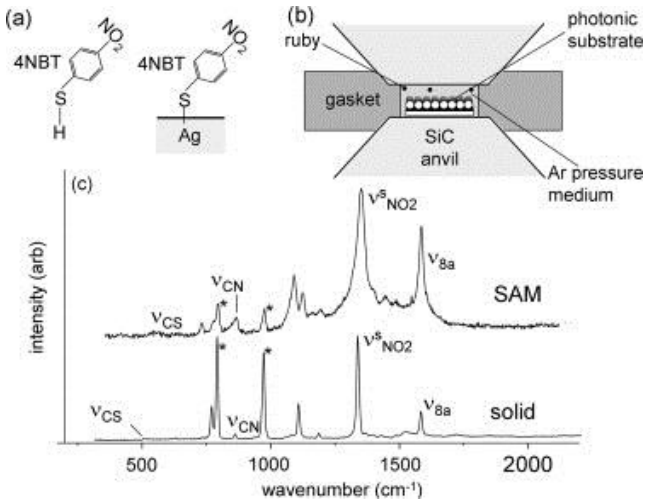


**Figure 4.1**

a) Approximate configuration of 4-nitrobenzenethiol (NBT) molecule and self-assembled monolayer (SAM). (b) Schematic of SiC anvil high-pressure cell with ruby pressure sensors and photonic substrate for surface-enhanced Raman scattering from SAMs. (c) Raman spectra of NBT in the solid and as a SAM, at a lower pressure of ~0.2 GPa, with assignments of four prominent transitions. The * denote transitions of the SiC anvils.

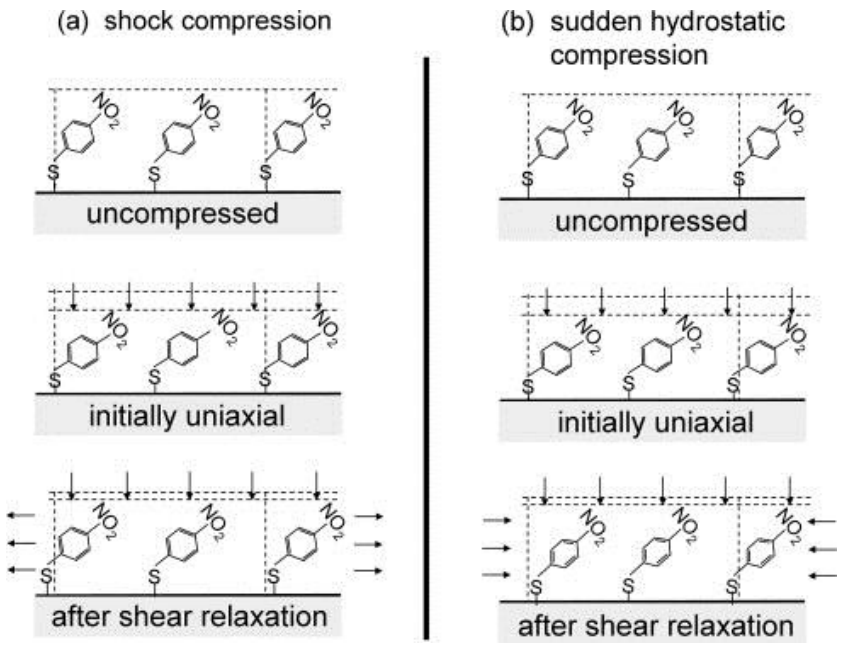


**Figure 4.2**

Schematic of the response of NBT SAM to (a) sudden shock and (b) sudden hydrostatic compression. Quasi 1D shock compression produces an initial state of uniaxial compression parallel to the surface normal. A subsequent shear relaxation can occur, caused by molecules moving outward parallel to the metal surface, converting part of the uniaxial strain to a transverse strain. Because the metal substrate is largely incompressible, a sudden hydrostatic compression also induced an initial uniaxial strain. A subsequent shear relaxation could result from molecules moving inward.

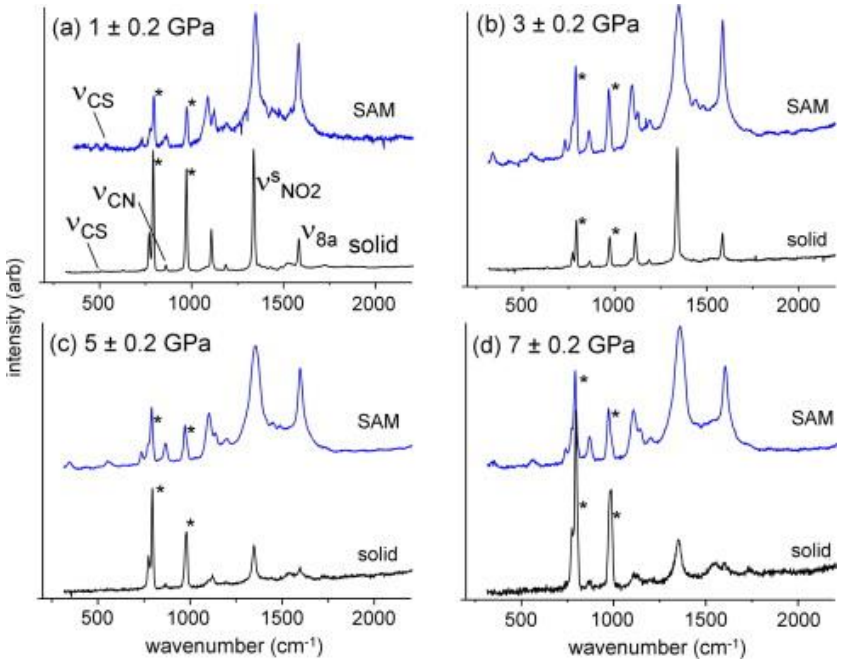


**Figure 4.3**

Raman spectra of NBT SAM on a photonic substrate with Ag(1 1 1) surface layer or as a neat solid. Transitions of the SiC anvil are indicated by *.

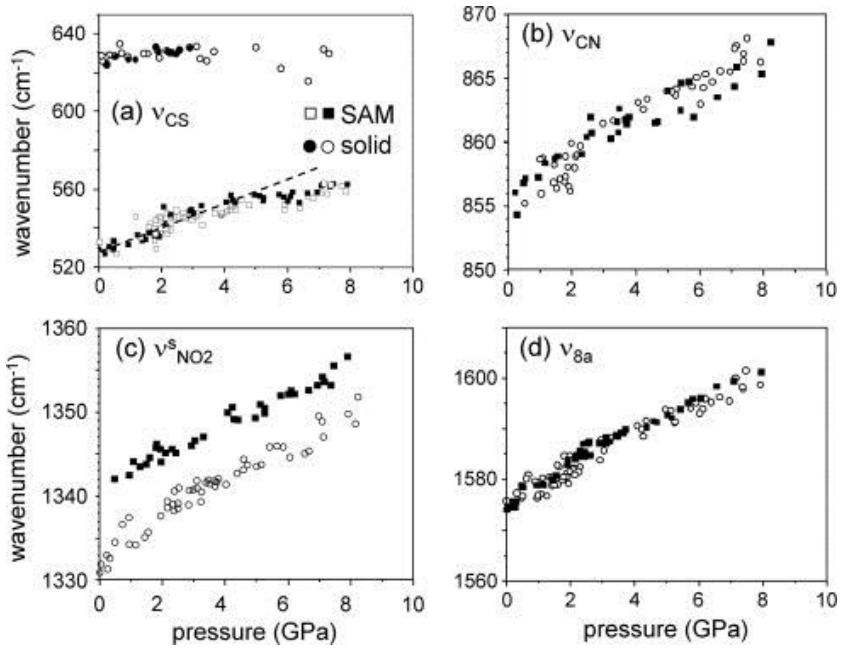


**Figure 4.4**

Pressure blueshifts of NBT SAM and solid for the four transitions indicated in Figure 4.1c. The line in a is a visual guide.

| Vibrational tranistion | Ambient ($cm^{-1}$) | $d\nu/dP$ ($cm^{-1}GPa^{-1}$) | $d\ln\nu/dP$ ($GPa^{-1}$) |
|---|---|---|---|
| $\upsilon CS^{a}$ | 538 | 7.0 | 0.013 |
| $\upsilon CN$ | 856 | 2.0 | 0.0023 |
| $\upsilon^{s}NO_2$ | 1331 | 2.1 | 0.0016 |
| $\upsilon 8a$ | 1574 | 3.4 | 0.0021 |

**Table 4.1**

Rate of pressure blueshift for nitrobenzenethiol SAM on Ag(1 1 1).

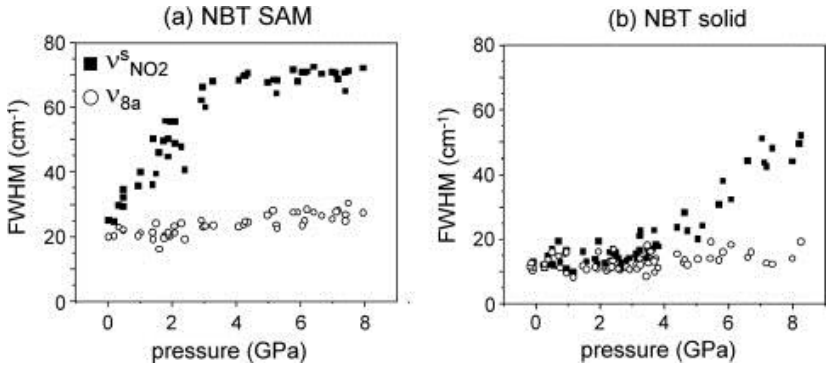


**Figure 4.5**

Pressure-dependent line broadening (FWHM) of the View the MathML source and ν8a transitions of NBT SAM and solid.

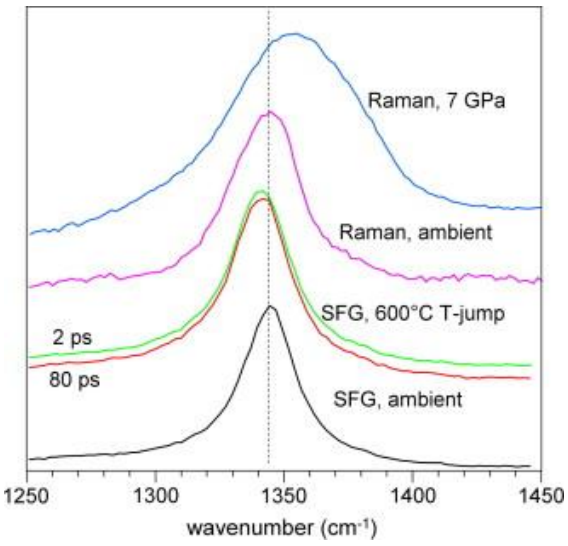


**Figure 4.6**

Spectra of View the MathML source transition of NBT SAM. Ambient spectra were obtained with both Raman and sum-frequency generation (SFG). With flash-heating a nonequilibrium population was observed at 2 ps. By 80 ps the SAM and surface are in equilibrium at 600 °C. The T-jump spectra, which are too fast for thermal decomposition or thermal expansion, show minimal redshift and broadening. At a high pressure of 7 GPa, the SAM shows a pressure blueshift and pressure broadening.

## 4.6 References


[1] D.D. Dlott, Annu. Rev. Phys. Chem. 50 (1999) 251.

[2] D.E. Hare, J. Franken, D.D. Dlott, Chem.Phys.Lett. 244 (1995) 224.

[3] N. Hemmi, Z.A. Dreger, Y.A. Gruzdkov, J.M. Winey, Y.M. Gupta, J. Phys. Chem. B 110 (2006) 20948.

[4] S.D. McGrane, D.S. Moore, D.J. Funk, J. Phys. Chem. A 108 (2004) 9342.

[5] J.E. Patterson, Z.A. Dreger, M. Miao, Y.M. Gupta, J. Phys. Chem. A 112 (2008) 7374.

[6] D.E. Hare, J. Franken, D.D. Dlott, J. Appl. Phys. 77 (1995) 5950.

[7] J.E. Patterson, A. Lagutchev, W. Huang, D.D. Dlott, Phys. Rev. Lett. 94 (2005) 015501.

[8] Z. Wang, J.A. Carter, A. Lagutchev, Y.K. Koh, N.-H. Seong, D.G. Cahill, D.D. Dlott, Science 317 (2007) 787.

[9] K.E. Brown, D.D. Dlott, J. Phys. Chem. C 113 (2009) 5751.

[10] J.A. Carter, Z. Wang, H. Fujiwara, D.D. Dlott, J. Phys. Chem. A 113 (2009) 12105.

[11] K.E. Lipinska-Kalita, M.G. Pravica, M. Nicol, J. Phys. Chem. B 109 (2005) 19223.

[12] P.F. Weck, C. Gobin, E. Kim, M.G. Pravica, J. Raman Spectrosc. 40 (2009) 964.

[13] M. Pravica, B. Yulga, Z. Liu, O. Tschauner, Phys. Rev. B 76 (2007) 064102.

[14] D.T. Cromer, R.R. Ryan, D. Schiferl, J. Phys. Chem. 89 (1985) 2315.

[15] G.J. Piermarini, S. Block, P.J. Miller, J. Phys. Chem. 93 (1989) 457.

[16] G.I. Pangilinan, Y.M. Gupta, J. Phys. Chem. 98 (1994) 4522.

[17] S. Courtecuisse, F. Cansell, D. Fabre, J.P. Petitet, J. Phys. IV France 5 (1995) C4359.

[18] S. Courtecuisse, F. Cansell, D. Fabre, J.P. Petitet, J. Chem. Phys. 102 (1995) 968.

[19] J.M. Winey, Y.M. Gupta, J. Phys. Chem. B 101 (1997) 10733.

[20] S. Courtecuisse, F. Cansell, D. Fabre, J.P. Petitet, J. Chem. Phys. 108 (1998) 7350.

[21] T. Kobayashi, T. Sekine, Phys. Rev. B 62 (2000) 5281.

[22] N. Kozu, M. Arai, M. Tamura, H. Fujihisa, K. Aoki, M. Yoshida, Japan J. Appl. Phys. 39 (2000) 4875.

[23] N. Kozu, T. Kadono, R.I. Hiyoshi, J. Nakamura, M. Arai, M. Tamura, M. Yoshida, Propell. Explos. Pyrotechn. 27 (2002) 336.

[24] A. Matsuda, H. Nagao, K.G. Nakamura, K. Kondo, Chem.Phys.Lett. 372 (2003) 911.

[25] S.D. McGrane, D.S. Moore, D.J. Funk, R.L. Rabie, Appl. Phys. Lett. 80 (2002) 3919.

[26] C.A. Bolme, S.D. McGrane, D.S. Moore, D.J. Funk, J. Appl. Phys. 102 (2007).

[27] Y.B. Zel'dovich, Y.P. Raizer, Physics of Shock Waves and High-Temperature Hydrodynamic Phenomena, Academic Presss, New York, 1967.

[28] H. Kim, S.A. Hambir, D.D. Dlott, Phys. Rev. Lett. 83 (1999) 5034.

[29] H. Kim, S.A. Hambir, D.D. Dlott, J. Phys. Chem. B 104 (2000) 4239.

[30] D.D. Dlott, M.D. Fayer, J. Chem. Phys. 92 (1990) 3798.

[31] A. Tokmakoff, M.D. Fayer, D.D. Dlott, J. Phys. Chem. 97 (1993) 1901.

[32] G. Tas, J. Franken, S.A. Hambir, D.E. Hare, D.D. Dlott, Phys. Rev. Lett. 78 (1997) 4585.

[33] A. Lagutchev, S.A. Hambir, D.D. Dlott, J. Phys. Chem. C 111 (2007) 13645.

[34] J.A. Carter, Z. Wang, D.D. Dlott, Acc. Chem. Res. 42 (2009) 1343.

[35] W.J. Evans, C.-S. Yoo, G.W. Lee, H. Cynn, M.J. Lipp, K. Visbeck, Rev. Sci. Instrum. 78 (2007).

[36] F. Schreiber, Prog. Surf. Sci. 65 (2000) 151.

[37] R.W. Carpick, M. Salmeron, Chem. Rev. 97 (1997) 1163.

[38] J.C. Bellows, P.N. Prasad, J. Chem. Phys. 70 (1979) 1864.

[39] R.M. Shelby, C.B. Harris, P.A. Cornelius, J. Chem. Phys. 70 (1979) 34.

[40] D.R. Jung, A.W. Czanderna, Critical Reviews in Solid State and Materials Sciences 19 (1994) 1.

[41] Z. Zhu, T.A. Daniel, M. Maitani, O.M. Cabarcos, D.L. Allara, N. Winograd, J. Am. Chem. Soc. 128 (2006) 13710.

# CHAPTER 5: SINGLE MOLECULE UNDER HIGH PRESSURE*

## 5.1 Introduction

Molecular vibrations under high pressure generally exhibit blueshifts and broadenings [1]. The blueshifts arise from anharmonic coupling between intramolecular vibrations and the environment [1,2]. Broadening originates from many sources, and although it is a substantial simplification, it is often satisfactory to describe broadening as homogeneous or inhomogeneous [3,4]. At ambient temperature, homogeneous broadening of vibrational transitions in solids arises primarily from "pure dephasing" caused by faster modulations of the vibrational frequency by the surroundings [3-7]. Inhomogeneous broadening results from each molecule in the ensemble having different slower interactions with the surroundings, i.e. each molecule possesses a unique slowly-changing or static structural environment [3]. By definition, single molecule Raman spectra should be homogeneously broadened [8,9]. In the present study, we used single-molecule surface-enhanced Raman scattering (SMSERS) [10-12] in a diamond-anvil cell (DAC) to investigate how these blueshifting and broadening processes are affected by increasing pressures up to 4 GPa, where volume compression is ~25%. We show that individual molecules have different pressure shifts, and these differential pressure shifts are the primary cause of the ensemble-averaged pressure-induced line broadening.

In these experiments, we used a well-studied system for SMSERS consisting of citrate-reduced colloidal Ag particles dosed with a probe dye molecule, Rhodamine 6G (R6G). The samples were in the form of ~200 x 200 x 20 $\mu m^3$ chips in the DAC, consisting of the dosed colloid suspended in a polymer matrix. The chips in the DAC were surrounded by supercritical

* Adapted with permission from Journal of Physical Chemistry C. Copyright 2015 American Chemical Society.

Ar. This pressure medium produces hydrostatic compression up to 10 GPa [13]. The DAC was inserted either in a 532-nm Raman spectrometer for surface-enhanced Raman (SERS) ensemble studies, or a 532-nm scanning Raman confocal microscope for SMSERS.

A technique that helps assure that SMSERS measurements are truly probing single molecules uses two isotopologues, R6G (natural abundance R6G) and $d_4$-R6G, where the phenyl group attached to the xanthene moiety is deuterated [14]. R6G has a vibrational transition near 610 $cm^{-1}$, which we shall term the "isotope-sensitive" transition, and it represents a ring deformation of the phenyl group. The isotope-sensitive transition has a noticeable shift between the two isotopologues, 610 $cm^{-1}$ in R6G and 602 $cm^{-1}$ in $d_4$-R6G at ambient pressure. If a proposed-SMSERS spectrum shows both isotopologues, it clearly does not originate from a single molecule. But if it is a "single-isotope" spectrum, it most likely originates from a single molecule.

It turns out that the isotope-sensitive transition has only a minimal pressure shift, so to study pressure-blueshifting in R6G, we focused on a transition near 1650 $cm^{-1}$, nominally an in-plane stretching mode of the xanthene moiety, which had a prominent pressure shift of ~5 $cm^{-1}$ $GPa^{-1}$. We will call this the "pressure-sensitive" transition. And we will show that Raman spectra and pressure-induced blueshifts of this transition were nearly identical for the two R6G isotopologues. In a 2014 conference proceeding [15], we reported a significant and partially permanent reduction of R6G SERS intensities in a DAC, whenever pressure was increased above ambient. We also reported the ensemble-averaged shift of the pressure-sensitive transition in R6G, and the near pressure-insensitivity of the isotope-sensitive transition from 0 to 6 GPa. Although Raman scattering of materials at high pressures in a DAC have become commonplace

[16], here we provide what are, to our knowledge, the first SMSERS measurements in a DAC, along with additional ensemble SERS data needed to support the SMSERS measurements.

Performing SMSERS measurements in a DAC in the GPa pressure range caused difficulties that forced us to modify some of the conventional methods usually employed in SMSERS experiments [10,14]. We immobilized the R6G-dosed Ag colloidal nanoparticles in a polymer film, poly vinyl alcohol (PVA), chosen for its water solubility and compatibility. A chip of PVA could then be inserted into the small (400 μm diameter x 75 μm) sample chamber of the DAC and surrounded by the Ar pressure medium. Only a small fraction of SERS-active hotspots survive GPa pressures, so it was necessary to employ higher particle densities and dye doses than are typically used [14].

Because the DAC had to be removed from the spectrometer or Raman microscope for pressure adjustments, the position registration was lost as the pressure was tuned. As a result, we were unable to track the evolution of a specific hot spot under increasing pressure. In order to resolve isotope splitting and pressure-induced blueshifting, we utilized the highest resolution grating available, which provides a spectral resolution of 2-3 $cm^{-1}$. However, the bandwidth at this resolution (440-500 $cm^{-1}$) did not cover both the isotope-sensitive and pressure-sensitive transitions. Thus, the spectrograph had to be tuned between the pressure- and isotope-sensitive regions, which created a time delay (10 s) and required mechanical movement of the optics. These two problems created the potential loss of spatial correspondence between spectra in the isotope-sensitive region and spectra in the pressure-sensitive region. Thus we collected separate scans of spectra from the isotope-sensitive region and the pressure sensitive region. When the majority of the isotope-sensitive transitions were single-molecule at a certain pressure, we assumed that was true as well for the pressure-sensitive transition.

## 5.2 Experimental

### 5.2.1 Sample preparation

Sample preparation procedure was described in chapter 2.

### 5.2.2. Diamond anvil cell

The diamond anvil cell and operation procedures have been described in Chapter 3. The sample chips were loaded into the DAC along with 4-8 ruby chips surrounding the sample, as seen in Fig. 5.1a, in order to obtain a precise measurement of the pressure and to monitor possible pressure gradients. From 0 to 4 GPa, the maximum experimental errors and variances of the pressures within the cell, based on the fluorescence from the 4-8 individual ruby chips, were 0.1 GPa.

### 5.2.3. Raman apparatus

The Raman apparatus was described in Chapter 3. The excitation laser was 1 mW at 532 nm, focused to ~30 μm diameter. The spectral resolution, determined by the response to atomic emission lines, was 10 $cm^{-1}$ FWHM. This apparatus was also used for absorption and extinction measurements in the DAC, using a fiber-coupled tungsten-halogen white light source and a fiber-coupled spectrograph (Ocean Optics). The focused spot size of the white light was small enough that all the white light passed through the PVA chip.

The Horiba LabRAM HR confocal Raman imaging microscope has been described in Chapter 3. We estimated the scattering volume to be 25 $\mu m^3$. Assuming a mean particle size of 35-50 nm [14,17] and knowing the Ag content of the sample, we estimated the number of colloidal particles in the scattering volume to be, on average, 200-600.

During data acquisition, the DAC was scanned in the *xy* plane with a step size of 4 μm. The data collection time was 10 s per spectrum. Each scan yielded about 2500 spectra. In the 350 $cm^{-1}$ to 850 $cm^{-1}$ range used to study the isotope-sensitive transition, the spectral resolution was 3 $cm^{-1}$. In the 1350 $cm^{-1}$ to 1790 $cm^{-1}$ range used to study the pressure-sensitive transition, the spectral resolution was 2 $cm^{-1}$.

The software used to control the confocal Raman microscope output a .txt file containing the wavenumber, the digitized brightness level of each pixel, and the *xy* coordinates. All spectra were screened by a Peakfinder [18] routine to discard those without recognizable Raman transitions. Spectra containing identified peaks were fitted to a Lorentzian to extract the Raman wavenumber, intensity and linewidth using a custom Matlab (MathWorks) script (Appendix A). The use of a Lorentzian is not intended to indicate any *a priori* knowledge of the lineshape; it was simply an artifice to determine reliable peak locations and FWHM.

**5.3 Results**

Figure 5.2 shows SERS (ensemble) spectra of R6G at ambient and elevated pressures, with the isotope-sensitive and pressure-sensitive transitions indicated by arrows. The data in Fig. 5.2a were reproduced from reference [15]. The reduction of SERS intensities with high pressure can be seen by comparison to the approximately constant intensity of the diamond transition near 1332 $cm^{-1}$. After a cycle of increasing the pressure to 6.2 GPa and then decreasing it back to ambient, the SERS intensity recovered significantly, but a nonrecoverable permanent intensity loss of approximately a factor of two was seen [15].

The extinction spectra, which arise mainly from the plasmon resonances of the Ag colloid, are shown in Fig. 5.2b. Compressing the sample causes the extinction intensity (i.e. the

attenuation of white light) to decrease. Releasing the compression causes some but not all of the intensity to recover. There is no significant pressure-induced frequency shift of the extinction spectrum.

The SERS results for the pressure shifts, intensities and linewidths (expressed as full-width half maxima, FWHM) for the pressure-sensitive transition are shown in Fig. 5.3. These results are in good agreement with our previously published study [15]. The shifts and intensities of the isotope-sensitive transition are shown in Fig. 5.4. The SERS intensities dropped precipitously after the minimum measureable pressure (0.1-0.2 GPa) was applied. The pressure-sensitive transition (Fig. 5.3) blueshifted by about 30 $cm^{-1}$, and its linewidth approximately doubled, from 17 to 30 $cm^{-1}$, as pressure was increased from ambient to 6.2 GPa. In the same pressure range, the isotope-sensitive transition blueshifted hardly at all, by only ~3 $cm^{-1}$ (Fig. 5.4a).

Figures 5.1b-f show Raman images of a sample in the DAC at ambient pressure (Fig. 5.1b), at ambient pressure after loading to 4.1 GPa (Fig. 5.1f) and at a few high pressures (Figs. 5.1c-1e). The intensities of the bright spots are proportional to the intensities of the pressure-sensitive transition. Pressure caused the number of SERS-active hotspots to decrease markedly. But the remaining hot spots gave SMSERS spectra that were similar in intensity to the ambient SMSERS spectra. High pressure destroyed most of the hot spots, but those that survived had about the same enhancement factor as before.

Figure 5.5 shows some single-molecule spectra of the isotope-sensitive transition of R6G and $d_4$-R6G mixtures at 1GPa (30 nM of each isotopologue) and 2 GPa (60 nM of each). These spectra demonstrate that we can resolve the two isotopologues at higher pressures, so we can

clearly discern single-isotope hotspots, corresponding to likely single-molecule hotspots, in the DAC at GPa pressures.

In Fig. 5.6, we plot histograms of the frequency of observations of single-isotope and multiple-isotope spectra at different pressures, from spectra obtained using 30 nM and 60 nM of each isotopologue. With the 30 nM sample, close to ambient pressure (0.2 GPa) we observed 758 single-isotope spectra and 199 multiple-isotope spectra. Thus in the 0.2 GPa spectra, 79% of the spectra were single-isotope. At 1.0 GPa with the 30 nM dose, the number of spectra observed fell dramatically, from 957 to 59, but 85% of the observed spectra were single-isotope. With the 60 nM spectra, at 1 atm the multiple-isotope spectra dominated, with 90% of the spectra showing both isotopologues. At 1.0 GPa, the fraction of multiple-isotope spectra decreased to 59%. At 2.0 GPa and above, single isotope spectra predominated. For example, at 2.0 GPa, 67% of the spectra were single-isotope, and the percentage of single-isotope spectra increased even further at higher pressures. In future discussions, we will use results from 30 nM samples in the 0-1 GPa range and the 60 nM samples in the 2-4 GPa range.

The results in Figs. 5.1 and 6 show that going to higher pressure reduces the number of hot spots, but that we can partially overcome that by increasing the dye concentration. In order to better understand the origin of the SERS intensity reduction, we investigated the pressure redshift of the dye electronic absorption spectrum and its relation to the laser excitation wavelength that determines the extent of resonant Raman enhancement. Direct measurements of the absorption redshift of dye adsorbed on Ag colloid in a DAC were impossible due to the small number density. In this case, our best means of quantifying the absorption shift was to measure the absorption of a uniform solution of R6G in PVA where the peak absorbance was about unity.

Figure 5.7a shows that the peak frequency of the R6G $S_0 \rightarrow S_1$ transition redshifted by 20 nm from 1 atm to 4 GPa.

Figures 5.7b,c show the frequency of observing SMSERS spectra at different pressures using either the usual 532 nm laser or a 633 nm laser. With both excitation lines, the frequency decreased significantly when pressure was applied. This was despite the fact that pressure caused the absorption maximum to shift away from the 532 nm line and toward the 633 nm line (Fig. 5.7a).

The linewidths of the pressure-sensitive transition did not depend on whether the sample consisted of R6G alone or whether it was a mixture of R6G and $d_4$-R6G, presumably because the pressure-sensitive transition has little amplitude on the deuterated phenyl group. This result is illustrated in Fig. 5.8, where we plotted the ensemble-average spectra of the pressure-sensitive transition from 0-3 GPa. These spectra were obtained by averaging typically 20-200 SMSERS spectra. The linewidths in Fig. 5.8 were a bit narrower than in the SERS data in Fig. 5.2, because the SMSERS spectrometer had higher resolution (3 $cm^{-1}$) than the SERS spectrometer (10 $cm^{-1}$). This result indicates that we can combine linewidth and shift results from both pure R6G and R6G + $d_4$-R6G in our single-molecule studies of pressure tuning.

Figure 5.9 shows some examples of the narrowest SMSERS spectra of the pressure-sensitive transition at 2.0 GPa and 4.1 GPa. These narrower linewidths, in the 5.9 to 9.9 $cm^{-1}$ FWHM, were dramatically smaller than the SERS (ensemble) linewidths of 18 $cm^{-1}$ FWHM at 2.0 GPa and 21 $cm^{-1}$ FWHM at 4.1 GPa (seen in Fig. 5.3b). Each spectrum in Fig. 5.9 has more than 67% likelihood of being single-isotope, and are thereby statistically likely to be predominantly single-molecule. That conclusion is further reinforced by the linewidths being so much narrower than the ensemble measurements. When we computed the ensemble average of

the SMSERS spectra, shown at the top of Fig. 5.9, the resulting linewidths were close to the ensemble SERS results. The SMSERS linewidths were usually 2-3 $cm^{-1}$ narrower than the SERS linewidths due to the higher resolution of the SMSERS spectrograph.

We can determine the statistical distribution of SMSERS linewidths in the 1.0 - 4.1 GPa range for the pressure-sensitive transition, as shown in Fig. 5.10. There is hardly any or possibly no pressure broadening of these primarily single-molecule spectra. The statistically averaged linewidths were about the same at all pressures. In the 2.0, 2.8 and 4.1 GPa spectra, where we used the higher 60 nM R6G doses, there were a few lines that were quite a bit broader (25-30 $cm^{-1}$) than the ensemble average. We believe these broader transitions might indicate multiple-molecule sites.

Figure 5.9 suggests that different single-molecule spectra have different pressure-induced blueshifts. In order to quantify the distribution of the SMSERS blueshifts for the pressure-sensitive transition, in Fig. 5.11 we have plotted these statistical distributions for pressures in the 1-4 GPa range and fit them to Gaussian distributions. Figure 5.11 shows that higher pressure caused a blueshift and an increase in the variance of the distribution of SMSERS vibrational frequencies.

## 5.4 Discussion

### 5.4.1 SERS and SMSERS intensities under pressure

The SERS intensity dropped precipitously when the DAC was put under pressure (Figs. 5.3 and 5.4). As may be seen in Figs. 5.1b-e, SMSERS measurements tell us that the intensity loss is caused by a decrease in the number of SERS-active hot spots. The hot spots that remained at high pressures gave about the same SMSERS intensities as ambient-pressure hot

spots. The pressure-induced decrease in the number of hot spots could be partially overcome by boosting the R6G dose, but the higher doses cannot be used at lower pressures because too many of the spectra would not be single-molecule.

It is known that field enhancement via surface plasmon resonances and the resonance Raman effect both contribute to the huge Raman cross-sections of R6G needed for SMSERS [11,19,20]. Figure 5.2b shows that the extinction spectrum attributed to the Ag colloid plasmon resonances decreases by about a factor of four at high pressures, but the extinction spectral peak does not shift. Figure 5.7 shows the pressure-induced redshift of the dye absorption maximum is uncorrelated with the number of hot spots observed. If the dye absorption redshift had a significant effect on SMSERS intensities, the redshifting of the absorption spectrum would cause the frequency of observing SMSERS spectra to increase with increasing pressure when 633 nm excitation was used, which was not observed (Fig. 5.7c). These observations indicate that the pressure-induced destruction of SMSERS hot spots results primarily from a process that reduces the SERS enhancements at most, but not all, hot spots.

In the absence of other plausible mechanisms, we believe pressure destroys hot spots and causes the extinction spectral intensities to decrease via configurational changes in the PVA-supported Ag colloid. We do not have compressibility data for PVA, but the compressibility ought to be similar to poly-methyl methacrylate (PMMA). Pressurizing PMMA to 0.2 GPa causes ~2.5% decrease in volume [21]. At 4 GPa the volume decrease is ~25%. Polymers such as PVA become permanently densified by high pressure, so part of the Ag colloid configurational changes would be permanent, which agrees with our observations that the number of hot spots is permanently decreased after a cycle of compression and decompression.

The hot spots in the Ag colloid are believed to result from Ag nanoparticle aggregates, especially dimers or trimers [22] having nanoscopic gaps [23] where R6G resides. The gap has to be very precise to provide the large enhancements needed for SMSERS [23], so it is easy to see how the strains introduced in a DAC could destroy hot spots. But it is not as easy to understand why compression did not create new hot spots to replace the ones it destroyed, for instance by compressing dimers having gaps a bit too big. On this question, we can only speculate. Perhaps the hot spots that were not destroyed under pressure have some PVA in the gaps that helps stabilize the gap spacing. The particles having too-large gaps might have enough PVA in the gap that pressure cannot create the needed gap spacing.

### 5.4.2 Blueshift and line broadening

Now we examine the mechanism of pressure-induced broadening and the closely-related issue of whether different single molecules have different blueshifts. Keep in mind that our multiple measurements of ruby fluorescence within the DAC preclude the existence of sizeable pressure gradients on the sample.

For the isotope-sensitive transition the answer is clear. The SERS data (Fig. 5.4a) show the isotope-sensitive transition has a small pressure-induced blueshift, less than 5 $cm^{-1}$ in 6 GPa. So for the isotope-sensitive transition, it is not possible to have much variation in the blueshift among individual single molecules.

For the pressure-sensitive transition, the SERS data in Fig. 5.3a shows a much larger blueshift, more than 30 $cm^{-1}$ over 6 GPa, and also a significant linebroadening. In the 0-6 GPa pressure range, the linewidth almost doubles. Now we look to the SMSERS results to understand the mechanisms. Figure 5.10 shows that the single-molecule linewidths do not

increase appreciably with pressure, so the homogeneous broadening, which is due to fast fluctuations of the vibrational frequencies, is not much affected by pressure [3-7]. In Fig. 5.12, we plot the ensemble linewidth from SERS measurements and the computed ensemble-average from multiple SMSERS measurements. These linewidths are about the same, although the SERS linewidths are systemically 2-3 $cm^{-1}$ larger due to the worse resolution of the SERS spectrograph. A linear fit to the pressure-induced linewidth increase gives 2.4 $cm^{-1}$/GPa. Also in Fig. 5.12 we have plotted the FWHM of the SMSERS distribution of vibrational frequencies. A linear fit to the pressure-induced linewidth increase gives a slope of 2.1 $cm^{-1}$/GPa. The close correspondence between these two slopes indicates that most (or possibly all) of the pressure-induced line broadening of the pressure-sensitive transition was due to variations of the individual molecular blueshifts.

**5.5 Summary and conclusions**

We studied SERS and SMSERS spectra of R6G on colloidal Ag particles immobilized in PVA matrix in the 0-6 GPa range, in a DAC. The SMSERS measurement were obtained under conditions where most spectra arise from single molecules, and by combining many SMSERS spectra we could compute ensemble-averaged spectra to compare to ensemble measurements using SERS.

There was a dramatic loss of SERS intensity when the samples were first put under pressure. The SMSERS results show this intensity loss resulted from pressure-induced destruction of most—but not all--of the SMSERS-active hot spots. Those hot spots that survived gave about the same single-molecule Raman intensities as the ambient-pressure hot spots. The Raman enhancement needed for SMSERS arises from plasmonic and resonance Raman

enhancements of the laser and Stokes Raman fields [11,20] Hot spot destruction was not caused by pressure tuning of the R6G absorption spectrum, so the process involves pressure reduction of the plasmonic enhancements of most (but not all) hot spots. Though we were not able to determine the precise mechanism, we attribute pressure-induced hot spot destruction to mechanical distortions of the gap junction induced by pressure-induced strain.

We studied two Raman transitions of mixed R6G-$d_4$-R6G samples, one near 610 $cm^{-1}$ termed the "isotope-sensitive" transition, and one near 1650 $cm^{-1}$ termed the "pressure-sensitive" transition. We used the isotope-sensitive transition to determine if SMSERS spectra were mostly single-isotope and therefore mostly single-molecule. The SMSERS spectra we observed were primarily single-molecule.

Analysis of the single-molecule spectra of the pressure-sensitive transition showed that the single-molecule Raman linewidths increased little with increasing pressure. The variations in the pressure-induced single-molecule blueshifts increased significantly with pressure. Thus for the pressure-sensitive transition, individual single molecules can have quite different pressure-shifting behavior, and the variations in blueshift among single molecules explain the pressure-induced broadening.

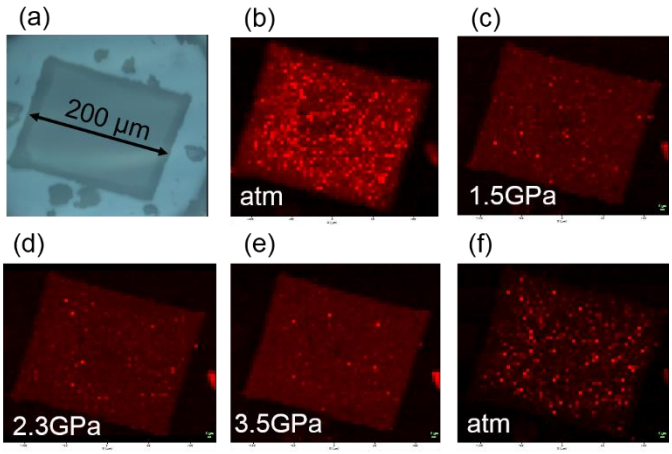


**Figure 5.1**

(a) Photo of a 200 x 200 x 20 $\mu m^3$ chip for SMSERS in DAC with Ar hydrostatic pressure medium. The eight surrounding spots are rubies for pressure calibration. (b)-(f) Raman microscope scans of the pressure-sensitive ~1650 $cm^{-1}$ R6G transition. The brightness of each pixel is proportional to the transition intensity. (b) Ambient pressure before loading Argon pressure medium. (c)-(e) With the DAC at the indicated pressures. (f) After 4 GPa pressure was applied and then released.

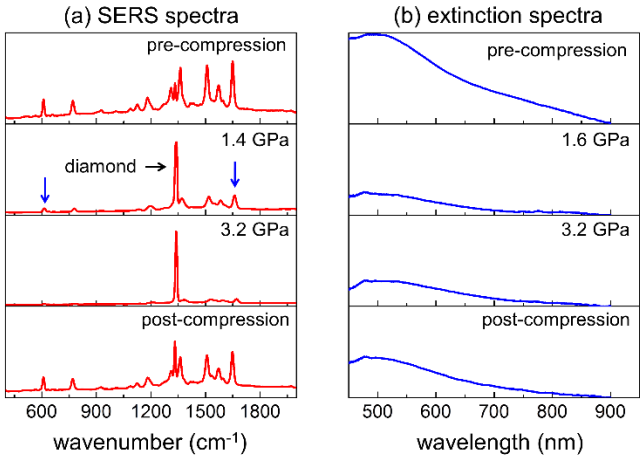


**Figure 5.2**

SERS spectra of R6G in a DAC. Note by comparison to the diamond transition how the SERS intensity decreased upon compression. The arrows indicate the locations of the isotope-sensitive (~610 $cm^{-1}$) and pressure-sensitive (~1650 $cm^{-1}$) transitions. (b) Extinction spectra (visible light attenuation) of the sample in a DAC. The extinction results mainly from plasmon resonances of the Ag nanoparticles. Reproduced from ref.15.

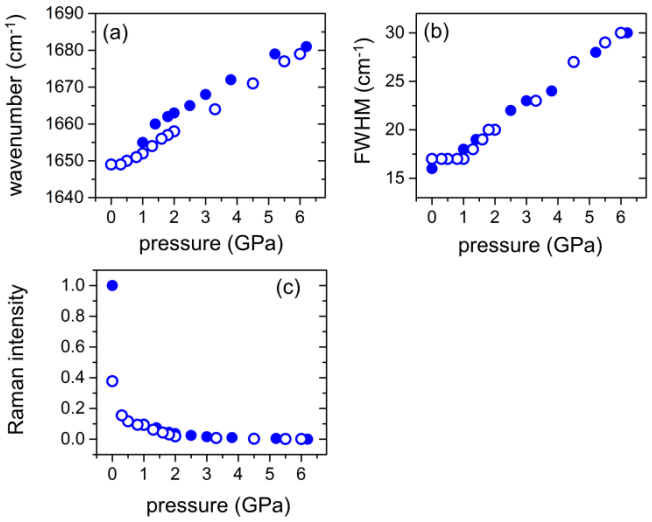


**Figure 5.3**

Pressure-induced blueshifts, broadening and intensities of the pressure-sensitive Raman transition of R6G from SERS (ensemble) measurements. Solid circles were obtained as the sample was compressed to ~6 GPa, and open circles as the sample was decompressed back to ambient.

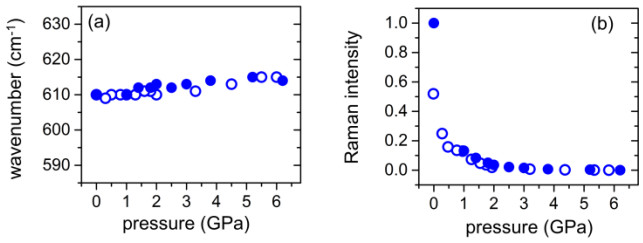


**Figure 5.4**

Pressure-induced blueshifts and intensities of the isotope-sensitive Raman transition of R6G from SERS (ensemble) measurements. Solid circles were obtained as the sample was compressed to ~6 GPa, and open circles as the sample was decompressed back to ambient.

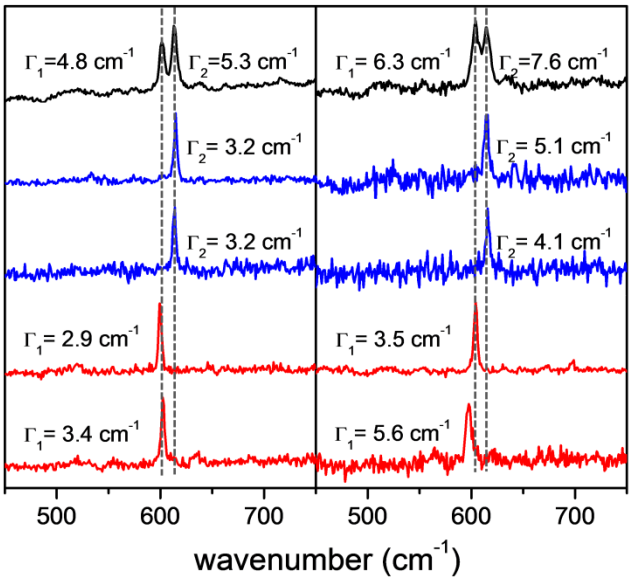


**Figure 5.5**

Some examples of SMSERS single-isotope spectra obtained at (a) 1 GPa (both isotopologues 30 nM ) and (b) 2 GPa (both isotopologues 60 nM). $\Gamma_1$ and $\Gamma_2$ are, respectively, the FWHM of the R6G and $d_4$-R6G isotope-sensitive transitions. The top spectrum in each panel is the computed ensemble average of many SMSERS spectra.

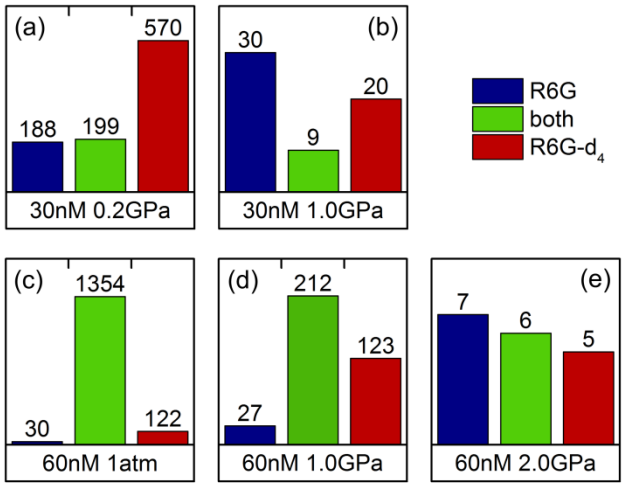


**Figure 5.6**

Histograms of the frequency of single-isotope spectra in SMSERS of isotopically-mixed R6G samples. The number of SMSERS spectra decreased when the samples were pressurized. The 30 nM (R6G + $d_4$-R6G) samples were predominantly single-isotope at 0.2 GPa (79% single-isotope) and 1.0 GPa (85% single-isotope). With 60 nM spectra, at 1 atm there were only 10% single-isotope spectra, but at 2 GPa and above, spectra were ≥67% single-isotope.

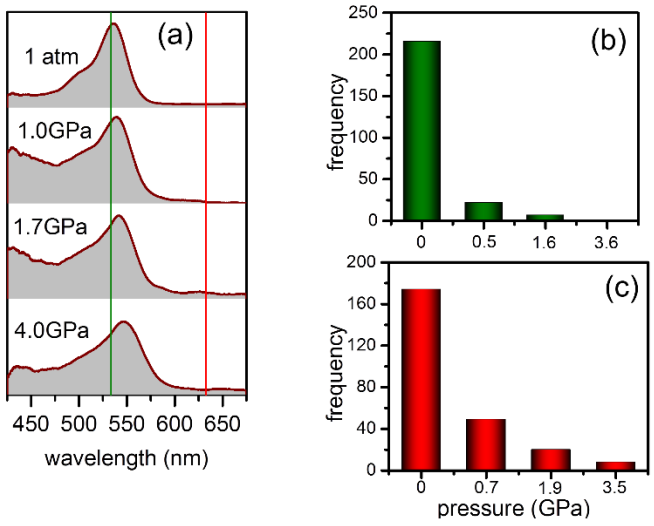


**Figure 5.7**

(a) Pressure tuned absorption spectra of R6G in PVA chip with 532 nm and 633 nm laser excitation lines indicated. (b) Frequency of observation of SMSERS spectra at different pressures using 532 nm excitation. (c) Frequency of observation of SMSERS spectra at different pressures using 633 nm excitation.

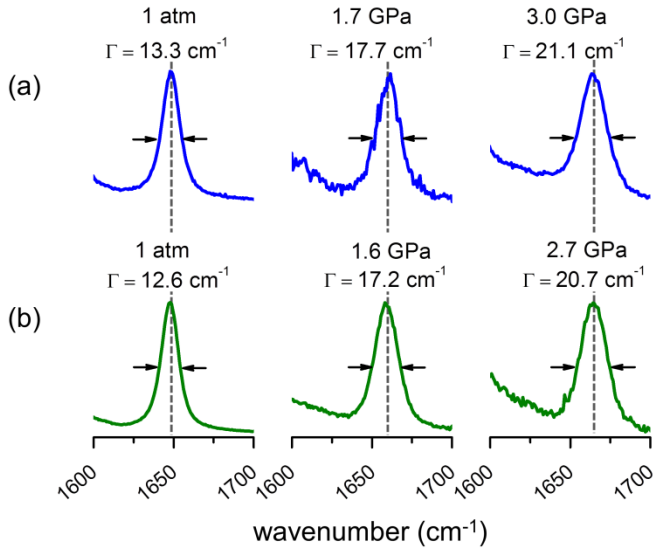


**Figure 5.8**

Ensemble averages of many SMSERS spectra for the pressure-sensitive transition (a) with R6G and (b) with R6G + $d_4$-R6G. For this transition, there were no significant differences in the peak locations or FWHM $\Gamma$ between R6G alone or R6G isotopic mixtures.

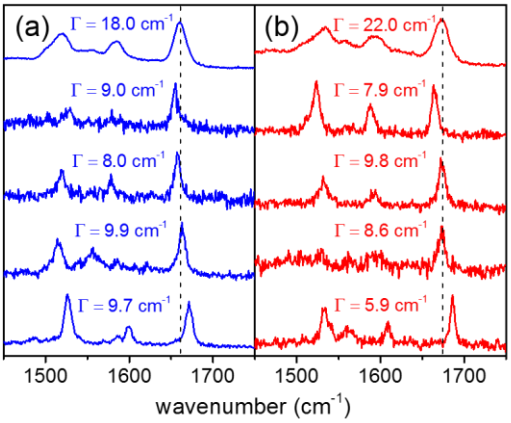


**Figure 5.9**

Some of the narrower SMSERS spectra of the pressure-sensitive transition at (a) 2.0 GPa and (b) 4.1 GPa. Γ is the FWHM. The uppermost spectra are computed ensemble averages. There are pressure-dependent variations in the SMSERS blueshifts of this transition that underlie the pressure broadening of the ensemble average.

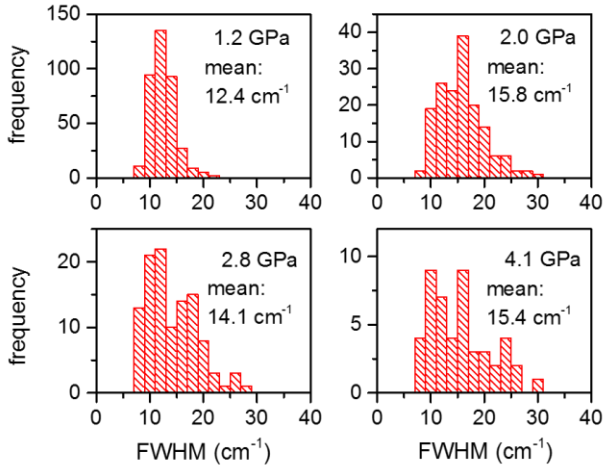


**Figure 5.10**

Histograms of the FWHM of SMSERS spectra of the pressure-dependent transition at 1.2 GPa (30 nM of each R6G isotopologue) and 2.0 to 4.1 GPa (60 nM of each). The single-molecule linewidths did not increase appreciably at higher pressures.

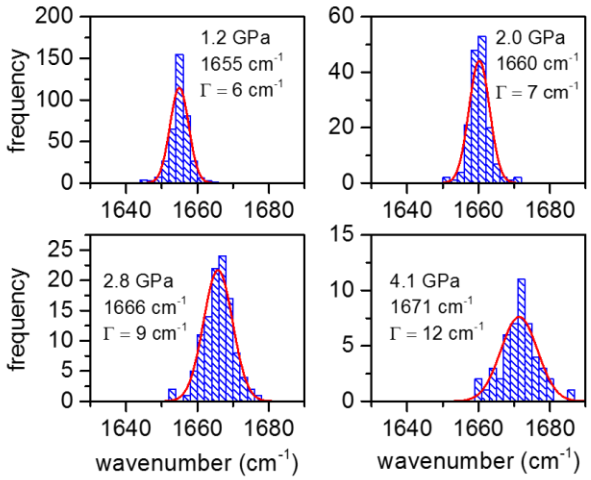


**Figure 5.11**

Histograms of the center frequencies of SMSERS spectra of the pressure-dependent transition at 1.2 GPa (30 nM R6G + 30 nM $d_4$-R6G) and 2.0 to 4.1 GPa (60 nM R6G + 60 nM $d_4$-R6G) . The blueshift variations (expressed as FWHM Γ of the distribution) increased with increasing pressure, showing that different single molecules have different pressure blueshifts.

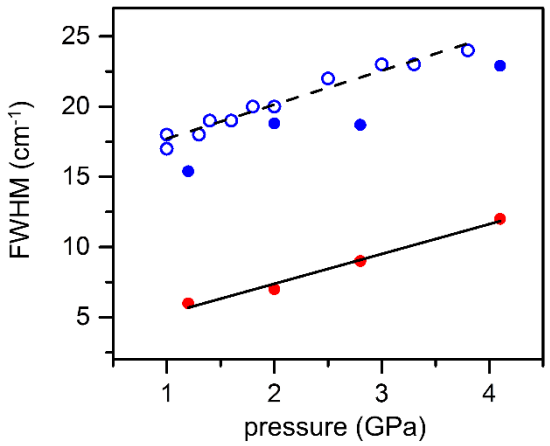


**Figure 5.12**

FWHM versus pressure of the pressure-sensitive transition from SERS measurements of the ensemble FWHM (open blue circles) and the computed ensemble average from SMSERS measurements. The SMSERS measurements were 2-3 $cm^{-1}$ narrower due to better spectroscopic resolution for the SERS spectrograph. The red circles are the FWHM of the frequency distribution obtained using single molecules. The rate of increase of the frequency distribution width matches the linewidth increase showing that different single molecules have different pressure-induced blueshifts and the variation of these blueshifts largely determines the pressure-induced line broadening.

## 5.6 References


[1] R.J. Hemley, Annu. Rev. Phys. Chem. 51 (2000) 763.

[2] G. Lucazeau, J. Raman Spectrosc. 34 (2003) 478.

[3] A. Tokmakoff, D. Zimdars, B. Sauter, R.S. Francis, R.S. Kwok, M.D. Fayer, *J. Chem. Phys* 101 (1994) 1741.

[4] A. Tokmakoff, M.D. Fayer, Acct. Chem. Res. 28 (1995) 437.

[5] C.L. Schosser, D.D. Dlott, J. Chem. Phys. 80 (1984) 1394.

[6] A. Tokmakoff, A. Kwok, U. Urdahl, D.A. Zimdars, R. Francis, M.D. Fayer, Laser Physics 5 (1995) 652.

[7] L.A. Hess, P.N. Prasad, J. Chem. Phys. 72 (1980) 573.

[8] P.G. Etchegoin, E.C. Le Ru, Analytical Chemistry 82 (2010) 2888.

[9] C. Artur, E.C. Le Ru, P.G. Etchegoin, J. Phys. Chem. Lett. 2 (2011) 3002.

[10] E.C. Le Ru, P.G. Etchegoin, Annu. Rev. Phys. Chem. 63 (2012) 65.

[11] S. Nie, S.R. Emory, Science 275 (1997) 1102.

[12] X.M. Qian, S.M. Nie, Chemical Society Reviews 37 (2008) 912.

[13] S. Klotz, J.C. Chervin, P. Munsch, G. Le Marchand, J. Phys. D-Appl. Phys. 42 (2009) 7.

[14] J.A. Dieringer, R.B. Lettan, K.A. Scheidt, R.P. Van Duyne, J. Am. Chem. Soc. 129 (2007) 16249.

[15] Y. Fu, J.M. Christensen, D.D. Dlott, J. Phys.: Conf. Ser. 500 (2014) 122004.

[16] A.F. Goncharov, Int. J. Spectrosc. 2012 (2012) 617528.

[17] A.M. Michaels, Jiang, L. Brus, J. Phys. Chem. B 104 (2000) 11965.

[18] N. Yoder, MATLAB Central File Exchange (2009).

[19] S. Shim, C.M. Stuart, R.A. Mathies, ChemPhysChem 9 (2008) 697.

[20] E.C. Le Ru, E. Blackie, M. Meyer, P.G. Etchegoin, J. Phys. Chem. C 111 (2007) 13794.

[21] H.F. Mark, N. Bikales, C.G. Overberger, G. Menges, J.I. Kroschwitz, Encyclopedia of Polymer Science and Engineering, Second Edition, Rapra Technology, Ltd., Shawbury, Shrewsbury, Shropshire, United Kingdom, 1985-1990.

[22] K.L. Wustholz, A.I. Henry, J.M. McMahon, R.G. Freeman, N. Valley, M.E. Piotti, M.J. Natan, G.C. Schatz, R.P. Van Duyne, J. Am. Chem. Soc. 132 (2010) 10903.

[23] J.M. McMahon, S. Li, L.K. Ausman, G.C. Schatz, J. Phys. Chen. C 116 (2011) 1627.

# CHAPTER 6: PRESSURE-TUNED LOCALIZED SURFACE PLASMON RESONANCE*

## 6.1 Introduction

Results obtained from single-molecule SERS study suggested that external pressure destroys the LSPR-based electromagnetic enhancement. Yet the mechanism remained uncertain. One way to characterize LSPR is by measuring the optical reflectance or extinction spectra of the substrate [1-5]. However, the extinction spectra of Lee-Meisel colloids are broad due to the heterogeneity in particle sizes and shapes, and limited information could be deduced from the measurement. In this chapter, we studied the pressure response of a photonic substrate consisting of Ag coated nano-sphere arrays (Fig 3.3). This photonic substrate has been used in previous studies to amplify Raman signal from self-assembled monolayers. Resonance frequency of the photonic substrate can be tuned by varying sphere size and Ag film thickness [3,6]. On the other hands, it is possible to simulate LSPR spectra based on size and shape of the nanostructure and the dielectric constants of the metal and surroundings [7-9]. Such capacity will help us to explain the pressure effect on LSPR. Measurements of the reflectance and Raman scattering were performed simultaneously at high pressure in a diamond anvil cell. The reflectance spectra reported changes in LSPR whereas the Raman scattering spectra of benzenethiol (BT) self-assembled monolayers reported the surface enhancement.

* Part of the materials presented in this chapter has been previously published in following article: Y. Fu, J.M. Christensen, D.D. Dlott, J. Phys.: Conf. Ser. 500 (2014) 122004. Published under license in Journal of Physics: Conference Series by IOP Publishing Ltd.

## 6.2 Experimental

Raman scattering and optical reflectance measurements were performed on a home-built Raman spectrometer. Details of the experiment apparatus and sample preparation procedure have been described in chapter 3.

## 6.3 Result and discussions

Some SERS spectra of BT SAM in the DAC are shown in Fig 6.1. We had previously studied the pressure-induced shifting of Raman transitions of the BT and other SAMs in a DAC. We found the adsorbate shifts were quite similar to molecules in a bulk solid and there was little hysteresis in the shift with increasing and decreasing pressures [10]. Now we have studied pressure effects on the LSPR spectra of the nano-sphere array, as shown in Fig 6.2. The LSPR has a broad resonance in the 450-675 nm range, with a peak at 620 nm (Fig 6.2a). Upon application of a small amount of pressure (0.7 GPa), dramatic changes in the LSPR spectra were observed. The LSPR resonance split into two peaks, at 500 nm and 750 nm, and neither peak had as much intensity as the original peak. Increasing the pressure to 6 GPa caused the two peaks to redshift, but continued pressure increase up to 6.9 GPa had minimal effect on the LSPR.

Figure 6.3 plotted the frequencies of the two resonance bands with respect to pressure. Both bands redshifted with increasing pressure. The higher-energy band shifted by approximately 50 nm up to 4 GPa, and remained nearly constant at higher pressures (Fig 6.3a). Since the silicon detector in the miniature spectrometer had poor efficiency beyond 900 nm, the lower-energy band above 5 GPa could not be tracked. However, between 0.7 to 5 GPa, the lower-energy band redshifted approximately 100 nm, twice of the higher-energy band (Fig 6.3b).

The frequency of LSPR depends on the size and geometry of the nanoparticles and the dielectric function of the metal and the surroundings. The LSPR will redshift if the nanoparticle size is increased, and blueshift if the size is decreased [11]. The redshift has been attributed to increased separation of image charges on opposite surfaces of the nanoparticles, which weakens the restoring force from the charges and lowers the LSPR frequency. In our case, at moderate pressure (0.7 GPa) where no phase transition exists, the dielectric function of metal (silver) and dielectrics, such as benzenthiol monolayer, argon and polystyrene, should change insignificantly [12-14] . A reasonable explanation to the abrupt change in LSPR spectra is that the forces exerted by the pressure medium on the Ag-coated polymer spheres deforms the spheres anisotropically, because only one-half of each sphere is in contact with the more incompressible Ag. The anisotropic compression breaks the radial symmetry, inducing new bands that were significantly shifted from the ambient pressure resonances.

The dielectric constant of dielectrics increase with density, and frequency of LSPR is seen to redshift with increased dielectric constant due to the build-up of polarization charges on the dielectric side, thus weakening the restoring force [15]. The red-shifts of both resonance bands above 0.7 GPa is likely to originate from the increased dielectric function. However, continuing structural deformation is another likely explanation.

The intensity evolution of four Raman active vibrational modes of benzenethiol were plotted in Fig 6.4. The Raman intensity increased by two folds from ambient pressure to 2 GPa but started to decrease gradually above 2 GPa. There were little hysteresis between 4 to 10 GPa, but the intensity plunged right below 4 GPa.

The increasing in the Raman intensity is attributed to the higher-energy LSPR band, which shifted from 620 to 500 nm and fortuitously remained in resonance with the laser and the

Stokes photons. The gradually decreasing in Raman intensity above 4 GPa was likely due to the monolayers, since the higher-energy band remained nearly constant above 4 GPa (Fig 3.3a). It is also interesting to notice the hysteresis in the Raman intensity, which is absent in the LSPR shifts. Either the change lead to plunging Raman intensity was associated with monolayer organization, or it occurred in the substrates but eluded the reflectance spectra measured in far-field.

## 6.4 Conclusions

We studied the effects of pressure the LSPR of a photonic substrate and the SERS spectra of benzenethiol self-assembled monolayers adsorbed upon. The pressure vibrational blueshifts of benzenethiol monolayers were unremarkable, but pressure effects on the LSPR spectra were significant. The nano-sphere array LSPR spectrum split into two peaks, presumably due to pressure-induced deformations of the polymer nanoparticles. Further redshifts of the two LSPR bands with increasing pressure may arise from continuing deformation or increased dielectric constant of the surrounding dielectric materials.

The pressure-tuned localized surface plasmon resonance has potential applications in high pressure Raman and local dielectric constant measurement. Future works can pursue a few directions. First is to carry out similar measurements on nano-spheres of different sizes. Secondly, we would like to find an internal Raman standard to obtain more precise measurement of the Raman intensity. The standard has to maintain constant Raman scattering intensity over a sufficiently wide pressure range. Quartz will be an option. Thirdly, we would like to perform electromagnetic calculations to explain the experimental results.

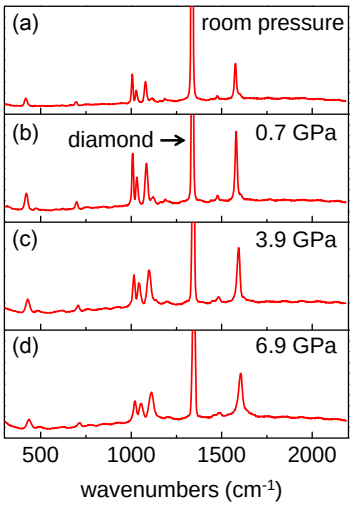


**Figure 6.1**

The SERS spectra of benzenethiol self-assembled monolayers on Ag-coated nanosphere arrays in a DAC.

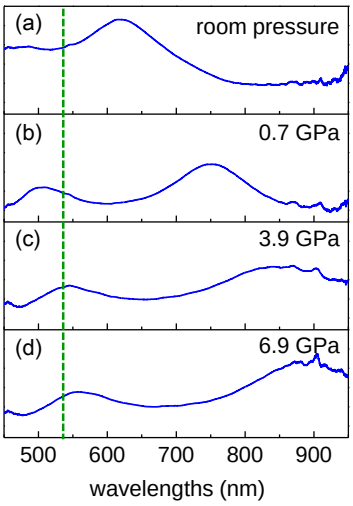


**Figure 6.2**

The LSPR spectra of Ag film coated nanosphere arrays. The green dashed line indicates the laser wavelength.

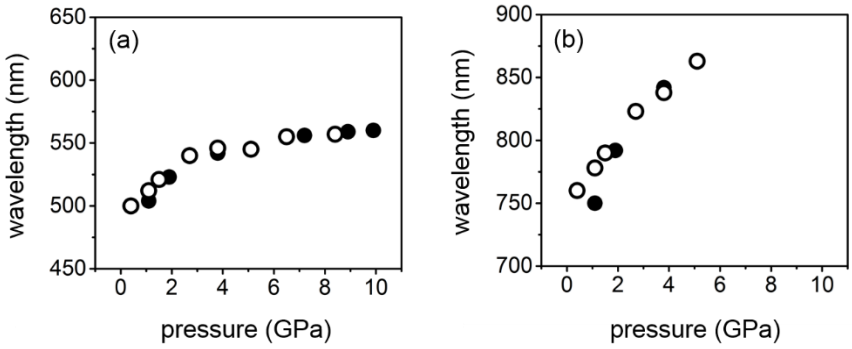


**Figure 6.3**

Pressure induced redshifts of the two localized surface plasmon resonances appeared upon initial compression. (a) The higher-energy band that was blueshifted (500nm) from the ambient pressure LSPR (620nm). (b) The lower-energy band that was redshifted (750nm) from the ambient pressure LSPR.

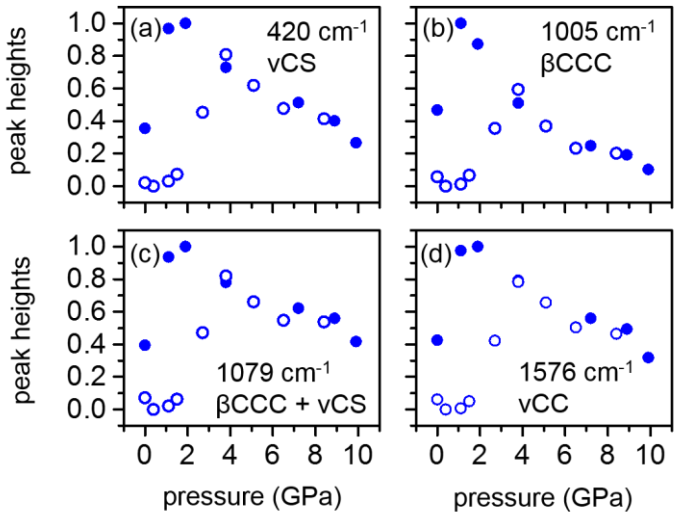


**Figure 6.4**

Normalized intensities of four Raman active vibrational modes of benzenthiol (BT) with respect to the static pressure. The highest intensity measured was set to unity.

## 6.5 References


[1] L. Baia, M. Baia, J. Popp, S. Astilean, The Journal of Physical Chemistry B 110 (2006) 23982.

[2] T.R. Jensen, M.D. Malinsky, C.L. Haynes, R.P. Van Duyne, J. Phys. Chem. B 104 (2000) 10549.

[3] W.C. Lin, L.S. Liao, H. Chen, H.C. Chang, D.P. Tsai, H.P. Chiang, Plasmonics 6 (2011) 201.

[4] J.M. Luther, P.K. Jain, T. Ewers, A.P. Alivisatos, Nat. Mater. 10 (2011) 361.

[5] J. Prikulis, P. Hanarp, L. Olofsson, D. Sutherland, M. Käll, Nano Letters 4 (2004) 1003.

[6] X. Zhang, J. Zhao, A.V. Whitney, J.W. Elam, R.P. Van Duyne, Journal of the American Chemical Society 128 (2006) 10304.

[7] B. Lamprecht, G. Schider, R.T. Lechner, H. Ditlbacher, J.R. Krenn, A. Leitner, F.R. Aussenegg, Physical Review Letters 84 (2000) 4721.

[8] L. Zhao, K.L. Kelly, G.C. Schatz, The Journal of Physical Chemistry B 107 (2003) 7343.

[9] C.L. Haynes, A.D. McFarland, L. Zhao, R.P. Van Duyne, G.C. Schatz, L. Gunnarsson, J. Prikulis, B. Kasemo, M. Käll, The Journal of Physical Chemistry B 107 (2003) 7337.

[10] K.E. Brown, D.D. Dlott, J. Phys. Chem. C 113 (2009) 5751.

[11] U. Kreibig, M. Vollmer, Optical properties of metal clusters, Springer-Verlag, 1995.

[12] R. Zallen, in: F. ABELES (Ed.), Optical properties and electronic structure of metals and alloys, North-Holland publishing company, Paris, 1966.

[13] J.F. Skinner, E.L. Cussler, R.M. Fuoss, J. Phys. Chem. 72 (1968) 1057.

[14] H. Sasabe, S. Saito, Polym J 3 (1972) 749.

[15] S.A. Maier, H.A. Atwater, J. Appl. Phys. 98 (2005) 10.

# Appendix A

## Matlab code "isotope-sensitive" vibrational transition

Input file: spectral data and calibration file
Output: number of single-R6G (612 $cm^{-1}$) spectra, number of single-R6G-d (602 $cm^{-1}$) spectra, number of both spectra

```
clear all

% Set up the frequency axis
a = 542.4466;
b = 0.0293;
flaser = 532.07;
x = 1:1:512;
wavelength = a + b.*x;
wavenumber = (1/flaser -1./wavelength).*10^7;
wavenumber = transpose(wavenumber);
save wavenumber.txt -ASCII wavenumber

clear all

sublb = 196;
subub = 296;
sublength = subub - sublb + 1;
spectralength = 512;
outputlength = spectralength + 3;

% calculate the subwavelength relation
a = 542.4466;
b = 0.0293;
bsub = b;
asub = a + (sublb-1)*b;
%end

offsetlb = -200;
offsetub = 200;
offsetic = 10.0;

% parameters for the peak fitting routine
R2threshold = 0.65;
WidthThresh = 0.5;
r6glb = 609;
r6gub = 619;
r6gdlb = 597;
r6gdub = 608;

% parameters for the peak finding routine
sel = 30;
thresh = 30;
ramanranges = [46 70];
r6g1 = 58;
r6g2 = 69;
```

```
r6gd1 = 47;
r6gd2 = 57;
%end

% all baseline fit settings
baserange1 = [1 127];
baserange2 = [462 512];
% end of baseline fit settings

% file organization
xstart = -110.0;
xend = 110.0;
ystart = -114.0;
yend = 114.0;
xstep = 4.0;
ystep = 4.0;
%end


% load the raw data, change name and location
load 141029S10.txt
% transfer data to variable 'data'
data = transpose(X141029S10);

%******************************
% do not modify anything bellow
%******************************

% count the number of hot sopts and errors

r6gcount = 0;
r6gdcount = 0;
bothcount = 0;
fitlabel = 0;
manualcounts1 = 0;
manualcounts2 = 0;

xdim = fix((xend-xstart)/xstep+1);
ydim = fix((yend-ystart)/xstep+1);

% number of datapoints for each file
datalength = xdim * ydim;

% output variables
bothfit = zeros(datalength,11);
r6gfit = zeros(datalength,11);
r6gdfit = zeros(datalength,11);
bothspectra = zeros(datalength,outputlength);
r6gspectra =  zeros(datalength,outputlength);
r6gdspectra = zeros(datalength,outputlength);
manualspectra1 = zeros(datalength,outputlength);
manualspectra2 = zeros(datalength,outputlength);


load wavenumber.txt
nwavenumber = wavenumber(sublb:subub,1);
```

```
% spectra fitting
for i = 1:datalength

    spectra = data(sublb:subub,i);

     % calculate the index
     [ylabel,xlabel] = indexcal(i,xdim,ydim,xstart,ystart,xstep,ystep);

    % subtract the baseline
    base1 = wavenumber(baserange1,:);
    base2 = wavenumber(baserange2,:);
    base3 = data(baserange1,i);
    base4 = data(baserange2,i);

    baselineWN = vertcat(base1,base2);
    baselineI = vertcat(base3,base4);

    p = TiltedBaselineFit(baselineWN,baselineI);
    base = p(1,1)*(1:1:spectralength)'+p(2,1);

    %create nspectra vector : the baseline subtracted data
    nspectra = spectra-base(sublb:subub,1);

    [peakloc,peakmag] = peakfinder(nspectra,sel,thresh,1,1);


    if isempty(peakloc)

    else
        peakcounts = histc(peakloc,ramanranges);
        numpeak = length(peakloc);
        peakmemo = zeros(2,2);

        if ge(peakcounts(1,1),3)

            % handle those spectra manually
            manualcounts1 = manualcounts1+1;
            manualspectra1(manualcounts1,1) = i;
            manualspectra1(manualcounts1,2) = ylabel;
            manualspectra1(manualcounts1,3) = xlabel;
            manualspectra1(manualcounts1,4:outputlength) =
transpose(data(:,i));

        elseif eq(peakcounts(1,1),2)

            for ipeak = 1:numpeak

                if ge(peakloc(ipeak,1),r6gd1) && le(peakloc(ipeak,1),r6gd2)
                    peakmemo(2,1) = peakloc(ipeak,1);
                    peakmemo(2,2) = peakmag(ipeak,1);
                end

                if ge(peakloc(ipeak,1),r6g1)&& le(peakloc(ipeak,1),r6g2)
                    peakmemo(1,1) = peakloc(ipeak,1);
```

```
                    peakmemo(1,2) = peakmag(ipeak,1);
                end

            end

                % fitting routine, fit as one peak or two peaks
                  r6gloc = asub + bsub * peakmemo(1,1);
                  r6gloc = (1/532.07-1/r6gloc)*10^7;
                  r6gdloc = asub + bsub * peakmemo(2,1);
                  r6gdloc = (1/532.07-1/r6gdloc)*10^7;
                  r6gmag = peakmemo(1,2)*pi*5.0/2.0;
                  r6gdmag = peakmemo(2,2)*pi*5.0/2.0;

                  bothlb = [0,r6glb,0,0,r6gdlb,0,offsetlb];
                  bothub = [inf,r6gub,20,inf,r6gdub,20,offsetub];
                  bothic = [r6gmag,r6gloc,2,r6gdmag,r6gdloc,2,offsetic];

                  coeff =
doublepeak(nwavenumber,nspectra,bothlb,bothub,bothic);

                 if (gt(coeff(1,7),R2threshold))

                    fitlabel = fitlabel + 1;
                    bothcount = bothcount+1;
                    bothfit(bothcount,1) = ylabel;
                    bothfit(bothcount,2) = xlabel;
                    bothfit(bothcount,3) = coeff(1,3);
                    bothfit(bothcount,4) = coeff(1,4);
                    bothfit(bothcount,5) = coeff(1,5);
                    bothfit(bothcount,6) = coeff(1,6);
                    bothfit(bothcount,7) = coeff(1,1);
                    bothfit(bothcount,8) = coeff(1,2);
                    bothfit(bothcount,9) = i;
                    bothfit(bothcount,10) = coeff(1,7);
                    bothfit(bothcount,11) =
coeff(1,1)/(coeff(1,1)+coeff(1,2));

                    bothspectra(bothcount,1) = i;
                    bothspectra(bothcount,2) = ylabel;
                    bothspectra(bothcount,3) = xlabel;
                    bothspectra(bothcount,4:outputlength) =
transpose(data(:,i));

                 end


        elseif eq(peakcounts(1,1),1)

             r6gflag = false;
             r6gdflag = false;

            for ipeak = 1:numpeak

                if ge(peakloc(ipeak,1),r6gd1) && le(peakloc(ipeak,1),r6gd2)
                    peakmemo(2,1) = peakloc(ipeak,1);
```

```
                    peakmemo(2,2) = peakmag(ipeak,1);
                    r6gdflag = true;
                end

                if ge(peakloc(ipeak,1),r6g1)&& le(peakloc(ipeak,1),r6g2)
                    peakmemo(1,1) = peakloc(ipeak,1);
                    peakmemo(1,2) = peakmag(ipeak,1);
                    r6gflag = true;
                end

            end

            % fit one peak
            if r6gflag

                  r6gloc = asub + bsub * peakmemo(1,1);
                  r6gloc = (1/532.07-1/r6gloc)*10^7;
                  r6gmag = peakmemo(1,2)*pi*5.0/2.0;

                coeff =
singlepeak(nwavenumber,nspectra,[0,r6glb,0,offsetlb],[inf,r6gub,20,offsetub],
[r6gmag,r6gloc,2,offsetic]);

              if (gt(coeff(1,5),R2threshold) && gt(coeff(1,3),WidthThresh))

                    fitlabel = fitlabel + 1;

                    r6gcount = r6gcount + 1;
                    r6gspectra(r6gcount,1) = i;
                    r6gspectra(r6gcount,2) = ylabel;
                    r6gspectra(r6gcount,3) = xlabel;
                    r6gspectra(r6gcount,4:outputlength) =
transpose(data(:,i));

                    r6gfit(r6gcount,1) = ylabel;
                    r6gfit(r6gcount,2) = xlabel;
                    % center freq
                    r6gfit(r6gcount,3) = coeff(1,2);
                    r6gfit(r6gcount,4) = 0.0;
                    % width
                    r6gfit(r6gcount,5) = coeff(1,3);
                    r6gfit(r6gcount,6) = 0.0;
                    % area
                    r6gfit(r6gcount,7) = coeff(1,1);
                    r6gfit(r6gcount,8) = 0.0;
                    r6gfit(r6gcount,9) = i;
                    r6gfit(r6gcount,10) = coeff(1,5);
                    r6gfit(r6gcount,11) = 1;

              end


            elseif r6gdflag

                  r6gdloc = asub + bsub * peakmemo(2,1);
```

```
                    r6gdloc = (1/532.07-1/r6gdloc)*10^7;
                    r6gdmag = peakmemo(2,2)*pi*5.0/2.0;


                coeff =
singlepeak(nwavenumber,nspectra,[0,r6gdlb,0,offsetlb],[inf,r6gdub,20,offsetub
],[r6gdmag,r6gdloc,2,offsetic]);

                if (gt(coeff(1,5),R2threshold)&& gt(coeff(1,3),WidthThresh))

                    fitlabel = fitlabel + 1;
                    r6gdcount = r6gdcount + 1;
                    r6gdspectra(r6gdcount,1) = i;
                    r6gdspectra(r6gdcount,2) = ylabel;
                    r6gdspectra(r6gdcount,3) = xlabel;
                    r6gdspectra(r6gdcount,4:outputlength) =
transpose(data(:,i));

                    r6gdfit(r6gdcount,1) = ylabel;
                    r6gdfit(r6gdcount,2) = xlabel;
                    % center freq
                    r6gdfit(r6gdcount,4) = coeff(1,2);
                    r6gdfit(r6gdcount,3) = 0.0;
                    % width
                    r6gdfit(r6gdcount,6) = coeff(1,3);
                    r6gdfit(r6gdcount,5) = 0.0;
                    % area
                    r6gdfit(r6gdcount,8) = coeff(1,1);
                    r6gdfit(r6gdcount,7) = 0.0;
                    r6gdfit(r6gdcount,9) = i;
                    r6gdfit(r6gdcount,10) = coeff(1,5);
                    r6gdfit(r6gdcount,11) = 0.0;
                end

            else
                manualcounts2 = manualcounts2+1;
                manualspectra2(manualcounts2,1) = i;
                manualspectra2(manualcounts2,2) = ylabel;
                manualspectra2(manualcounts2,3) = xlabel;
                manualspectra2(manualcounts2,4:outputlength) =
transpose(data(:,i));
            end

        end

    end
end

bothfit(all(~bothfit,2), : ) = [];
r6gfit(all(~r6gfit,2), : ) = [];
r6gdfit(all(~r6gdfit,2), : ) = [];
fittingresult = [bothfit;r6gfit;r6gdfit];
```

**Matlab code "pressure-sensitive" vibrational transition**

Input file: spectral data and calibration file
Output: The center frequency, intensity and FWHM of the three vibrational modes in this region

```
clear all

% Set up the frequency axis
a = 697.6109;
b = 0.0255;
flaser = 632.81;
x = 1:1:512;
wavelength = a + b.*x;
wavenumber = (1/flaser -1./wavelength).*10^7;
wavenumber = transpose(wavenumber);
save wavenumber.txt -ASCII wavenumber

clear all

a = 697.6109;
b = 0.0255;
flaser = 632.81;
sublb = 1;
subub = 512;
sublength = subub - sublb + 1;
spectralength = 512;
outputlength = spectralength + 3;


% file organization
xstart = -120.0;
xend = 120.0;
ystart = -90.0;
yend = 90.0;
xstep = 4.0;
ystep = 4.0;
%end

%define the peakfinder routine threshold
sel = 20;
thresh = 20;
ramanrange1 = [24 185];
ramanrange2 = [186 294];
ramanrange3 = [295 490];
ramanrangep1 = [84 162];
ramanrangep2 = [195 272];
ramanrangep3 = [342 427];

R2thresh = 0.8;
widththresh = 1.5;
avgwidth = 8;
%end

%set baseline paramters
base1 = 470;
```

```
base2 = 510;
baselength = base2-base1+2;

flag = 1;
comp = 10;


% load the raw data, change name and location
load 140716S6.txt
% Transfer the data to variable 'data'
data = transpose(X140716S6);

% call the dimension
xdim = fix((xend-xstart)/xstep+1);
ydim = fix((yend-ystart)/xstep+1);
datalength = xdim * ydim;
% end

load wavenumber.txt
nwavenumber = wavenumber(sublb:subub,1);

% initialize all the output variable
freqlog = zeros(datalength,15);
manuallog = zeros(datalength,1);
peak3log = zeros(datalength,5);
% end

%initializing all the parameters
manualcounts = 0;
freqcounts = 0;
cat1counts = 0;
cat2counts = 0;
cat3counts = 0;
cat1 = freqlog;
cat2 = freqlog;
cat3 = freqlog;

%end

for i = 1:datalength

    spectra = data(sublb:subub,i);

     % calculate the index
     [ylabel,xlabel] = indexcal(i,xdim,ydim,xstart,ystart,xstep,ystep);

    % calculate the baseline, average of first and last 'nbase' point
    base = sum(spectra(base1:base2,:))/baselength;

    %create nspectra vector : the baseline subtracted data
    nspectra = spectra-base+comp;

    [peakloc,peakmag] = peakfinder(nspectra,sel,thresh,1,1);

if ~isempty(peakloc)
```

```
    spec1 = 0;
    spec2 = 0;
    spec3 = 0;
    peak1 = zeros(1,10);
    peak2 = zeros(1,10);
    peak3 = zeros(1,10);
    peakmag1 = zeros(1,10);
    peakmag2 = zeros(1,10);
    peakmag3 = zeros(1,10);


     for j = 1:length(peakloc)

        if gt(peakloc(j,1),ramanrangep1(1,1)) &&
lt(peakloc(j,1),ramanrangep1(1,2))
            spec1 = spec1 + 1;
            peak1(1,spec1) = peakloc(j,1);
            peakmag1(1,spec1) = peakmag(j,1);
        end

        if gt(peakloc(j,1),ramanrangep2(1,1))&&
lt(peakloc(j,1),ramanrangep2(1,2))
            spec2 = spec2 + 1;
            peak2(1,spec2) = peakloc(j,1);
            peakmag2(1,spec2) = peakmag(j,1);
        end

        if gt(peakloc(j,1),ramanrangep3(1,1))&&
lt(peakloc(j,1),ramanrangep3(1,2))
            spec3 = spec3 + 1;
            peak3(1,spec3) = peakloc(j,1);
            peakmag3(1,spec3) = peakmag(j,1);
        end
    end

    if gt(spec1,1)||gt(spec2,1)||gt(spec3,1)
        manualcounts = manualcounts + 1;
        manuallog(manualcounts,1) = i;

    elseif eq(spec1,1)||eq(spec2,1)||eq(spec3,1)
        freqcounts = freqcounts + 1;
        freqlog(freqcounts,1) = i;
        freqlog(freqcounts,2) = ylabel;
        freqlog(freqcounts,3) = xlabel;
        flag = 1;

         if eq(peak1(1,1),0.0)
              freqlog(freqcounts,4) = 0;
              freqlog(freqcounts,5) = 0;
              freqlog(freqcounts,6) = 0;
              freqlog(freqcounts,7) = 0;
         else
              center = (1/flaser-1/(peak1(1,1)*b+a))*10^7;
              area = peakmag1(1,1)*pi*avgwidth/2;
              coeff =
```

```
singlepeak(wavenumber(ramanrange1(1,1):ramanrange1(1,2),:),nspectra(ramanrang
e1(1,1):ramanrange1(1,2),:),[0,(center-
20),0,0],[inf,(center+20),15,inf],[area,center,avgwidth,8]);
              if ge(coeff(1,5),R2thresh) && ge(coeff(1,3),widththresh)
              freqlog(freqcounts,4) = coeff(1,1);
              freqlog(freqcounts,5) = coeff(1,2);
              freqlog(freqcounts,6) = coeff(1,3);
              freqlog(freqcounts,7) = coeff(1,5);
              flag = 0;
              else
              freqlog(freqcounts,4) = 0;
              freqlog(freqcounts,5) = 0;
              freqlog(freqcounts,6) = 0;
              freqlog(freqcounts,7) = 0;
              end
         end


        if eq(peak2(1,1),0.0)
              freqlog(freqcounts,8) = 0;
              freqlog(freqcounts,9) = 0;
              freqlog(freqcounts,10) = 0;
              freqlog(freqcounts,11) = 0;
        else
              center = (1/flaser-1/(peak2(1,1)*b+a))*10^7;
              area = peakmag2(1,1)*pi*avgwidth/2;
              coeff =
singlepeak(wavenumber(ramanrange2(1,1):ramanrange2(1,2),:),nspectra(ramanrang
e2(1,1):ramanrange2(1,2),:),[0,(center-
20),0,0],[inf,(center+20),15,inf],[area,center,avgwidth,8]);
              if ge(coeff(1,5),R2thresh) && ge(coeff(1,3),widththresh)
              freqlog(freqcounts,8) = coeff(1,1);
              freqlog(freqcounts,9) = coeff(1,2);
              freqlog(freqcounts,10) = coeff(1,3);
              freqlog(freqcounts,11) = coeff(1,5);
              flag = 0;
              else
              freqlog(freqcounts,8) = 0;
              freqlog(freqcounts,9) = 0;
              freqlog(freqcounts,10) = 0;
              freqlog(freqcounts,11) = 0;
              end
        end


       if eq(peak3(1,1),0.0)
              freqlog(freqcounts,12) = 0;
              freqlog(freqcounts,13) = 0;
              freqlog(freqcounts,14) = 0;
              freqlog(freqcounts,15) = 0;
       else
              center = (1/flaser-1/(peak3(1,1)*b+a))*10^7;
              area = peakmag3(1,1)*pi*avgwidth/2;
              coeff =
singlepeak(wavenumber(ramanrange3(1,1):ramanrange3(1,2),:),nspectra(ramanrang
e3(1,1):ramanrange3(1,2),:),[0,(center-
```

```
20),0,0],[inf,(center+20),15,inf],[area,center,avgwidth,8]);
              if ge(coeff(1,5),R2thresh)&& ge(coeff(1,3),widththresh)
              freqlog(freqcounts,12) = coeff(1,1);
              freqlog(freqcounts,13) = coeff(1,2);
              freqlog(freqcounts,14) = coeff(1,3);
              freqlog(freqcounts,15) = coeff(1,5);
              flag = 0;
              else
              freqlog(freqcounts,12) = 0;
              freqlog(freqcounts,13) = 0;
              freqlog(freqcounts,14) = 0;
              freqlog(freqcounts,15) = 0;
              end
       end
      if flag
        freqcounts = freqcounts-1;
      end
    end
end

end

% Catagorize the spectra

for i = 1: freqcounts
    if gt(freqlog(i,4),freqlog(i,8)) && gt(freqlog(i,4),freqlog(i,12))
        cat1counts = cat1counts + 1;
        cat1(cat1counts,:) = freqlog(i,:);
    elseif gt(freqlog(i,8),freqlog(i,4))&&gt(freqlog(i,8),freqlog(i,12))
        cat2counts = cat2counts + 1;
        cat2(cat2counts,:) = freqlog(i,:);
    elseif gt(freqlog(i,12),freqlog(i,4))&&gt(freqlog(i,12),freqlog(i,8))
        cat3counts = cat3counts + 1;
        cat3(cat3counts,:) = freqlog(i,:);
    end
end
% end
```